AGU
ADVANCING
EARTH AND
SPACE SCIENCE

Tectonics

The Segmented Campo Felice Normal Faults: Seismic Potential Appraisal by Application of Empirical Relationships Between Rupture Length and Earthquake Magnitude in the Central Apennines, Italy

Giulia Schirripa Spagnolo[1], Marco Mercuri[1], Andrea Billi[2], Eugenio Carminati[1], and Paolo Galli[2,3]

[1]Dipartimento di Scienze della Terra, Sapienza Università di Roma, Rome, Italy, [2]IGAG, Consiglio Nazionale delle Ricerche, Rome, Italy, [3]Dipartimento della Protezione Civile Nazionale, Rome, Italy

Abstract During earthquakes, fault rupture can involve multiple segments in synchronous or cascade mechanisms, leading to an increasing magnitude of the mainshock or rate of aftershocks. Since the seismogenic portions of faults are inaccessible, studying the geometrical and mechanical interaction between exhumed fault segments can contribute to the understanding of multisegment and cascade earthquake scenarios at depth. We investigated a segmented active normal fault system in the Campo Felice area (central Italian Apennines), where fault scarps are well exposed. In this area, there are no instrumental-historical records of intermediate-strong earthquakes, although paleoseismology provided evidence for ancient $Mw > 5$ earthquakes. Geometry and kinematics of the studied faults as well as their physical linkage and mechanical interaction were assessed. Results of field surveys and geological-structural mapping, serial cross-sections, and throw versus distance diagrams highlight different stages of mechanical interaction between the Campo Felice faults. The suitability of three empirical equations relating earthquake rupture length and magnitude was tested in comparison to a new equation that we developed considering the last seven $Mw > 5.5$ earthquakes (1997–2016) from the central Apennines. Results show that the Campo Felice faults can produce earthquakes with maximum Mw of ∼5.8 and 6.2 with single or synchronous ruptures, respectively. In turn, Coulomb stress change modeling shows that the seismic hazard can increase considering a quasi-synchronous or cascade activation of the Campo Felice faults together with nearby faults.

1. Introduction

Recent seismological studies have highlighted different coseismic rupture scenarios. In some seismic sequences, the mainshock is followed by aftershocks having comparable magnitude. Significant examples are from Chile (2014–2015 seismic sequences, Mw 8.1–8.4; Papadopoulos & Minadakis, 2016) and Italy (2016; Mw 6.2–6.5; Chiaraluce et al., 2017; Figure 1a). In these cases, the slip on the fault segment causing the mainshock led to a stress transfer (i.e., Coulomb stress change; King et al., 1994; Stein, 2003; Tung & Masterlark, 2018) on nearby fault segments or patches from the same fault and hence to strong aftershocks or to a new larger mainshock. In these scenarios, the triggering delay times are generally in the order of 0.1–1 year (Scholz, 2010).

Coseismic deformation can also involve quasi-synchronous or cascade slip events over multiple adjacent fault segments during a single seismic event (Xu et al., 2018), all these contributing to the magnitude of the earthquake. The activation of multiple fault segments during an earthquake has been observed in several tectonic settings. For instance, under a strike-slip regime, the coseismic rupture during the 2016 Kaikoura earthquake (Mw 7.8, New Zealand) involved at least 21 fault segments for a total surface rupture length of about 180 km (Xu et al., 2018). The fault linkage caused a dramatic increase of the coseismic slip area and therefore of the released energy. Another significant example of multiple dynamic rupture is the 2012 Sumatra earthquake (Mw 8.6; Meng et al., 2012). The large magnitude of this earthquake resulted to be the consequence of the wide depth extent of the causative fault, high stress drop, and synchronous rupture of multiple fault segments that were oriented even orthogonally one to the other (Meng et al., 2012). Under extensional regime, three recent earthquake sequences in central Apennines (1997 Colfiorito, Mw 6.0;
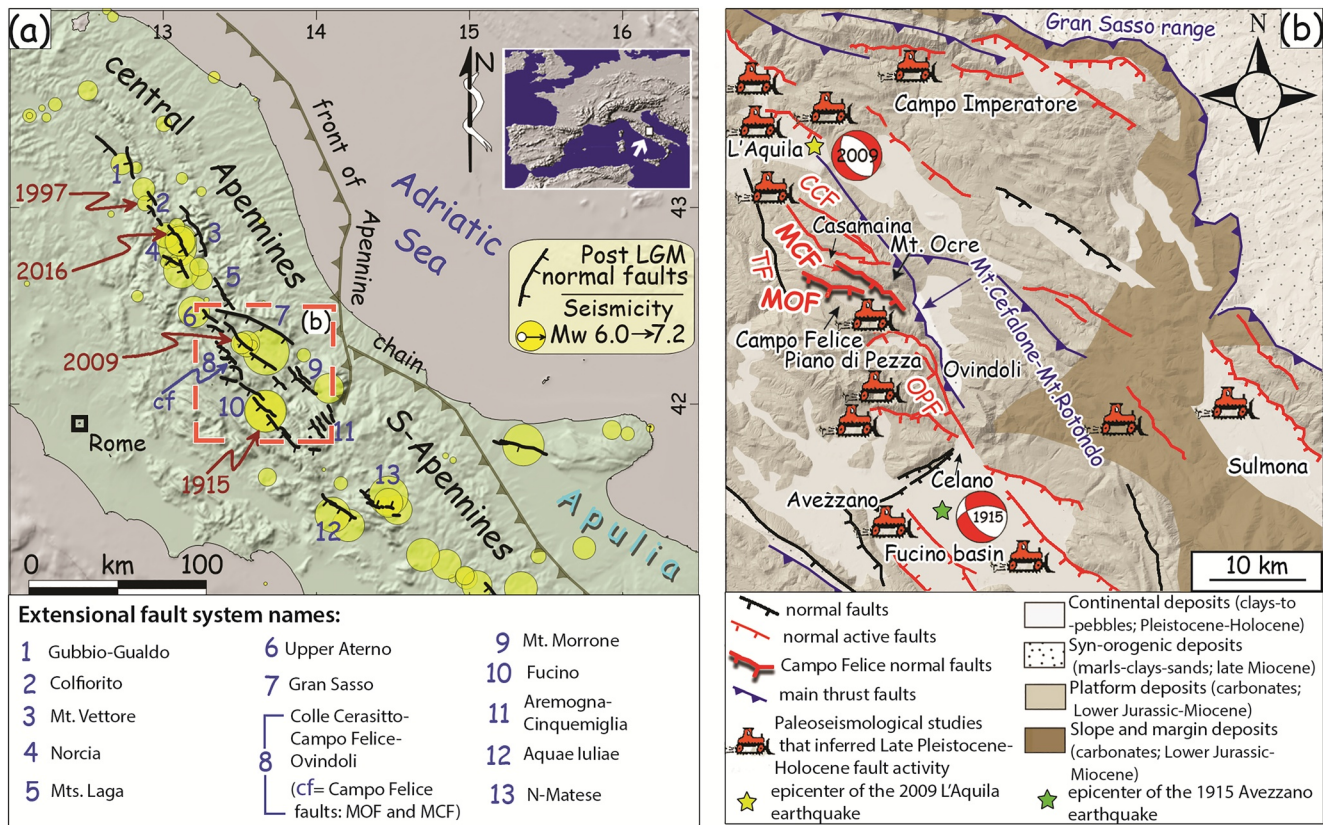
Figure 1. (a) Active faults and seismicity of the central Italian Apennines. The map reports the fault segments showing post-Last Glacial Maximum activity and the associated historical seismicity (dates refer to the main events of the last century). The dashed red box shows the location of the map of Figure 1b, which details the fault segments surrounding the study area. Inset: Location of study area within Europe. (b) The study area is characterized by compressive structures (blue in figure) such as the Mt. Cefalone-Mt. Rotondo thrust, and by normal faults (black in figure), some of them are inferred to be active (red in figure) by paleoseismological studies (Galli et al., 2008), that are indicated with bulldozers. The normal faults considered in this work are: Colle Cerasitto, Monte Cefalone (MCF), Monte Orsello (MOF), Tornimparte, and Ovindoli-Pezza faults. In this study, the Campo Felice faults include MOF and MCF. These two faults, which are the main subject of this work, border the Campo Felice basin. The yellow and green stars indicate the epicenters of the L'Aquila 2009 and Avezzano 1915 earthquakes, with their associated focal mechanisms (Galli et al., 2012). The different background colors show the main outcropping lithological successions (modified after Mercuri et al., 2020; Galli, 2020).

2009 L'Aquila, *Mw* 6.3; 2016 Amatrice-Norcia, *Mw* 6.0 and 6.5; Figure 1a) had mainshocks characterized by coseismic ruptures over several normal fault segments (Chiaraluce et al., 2003, 2011, 2017; Delorme et al., 2019; Iezzi et al., 2019; Pucci et al., 2019; Smeraglia et al., 2017). The Amatrice-Norcia sequence started on August 24, 2016, with a *Mw* 6.0 earthquake that ruptured the two adjacent tips of the Mt. Gorzano-Mt. Vettore fault. On October 26, a *Mw* 5.9 event ruptured the northernmost tip of the Mt. Vettore fault, whereas on October 30, a *Mw* 6.5 earthquake re-ruptured the whole fault, propagating along strike and involving slip over further fault segments (Brozzetti et al., 2019; Galli et al., 2019; Iezzi et al., 2019; Scognamiglio et al., 2018; Villani et al., 2018; Figure 1a).

In assessing the seismic potential of fault systems, adjacent fault segments should be considered collectively to test the possibility of their coseismic simultaneous activation (Brozzetti et al., 2019; Iezzi et al., 2019; Morell et al., 2020; Scotti et al., 2021; Sgambato et al., 2020; Walker et al., 2021; Wesnousky, 2008; Xu et al., 2018). The capability of coseismically breaking inter-segment barriers depends on the degree of mechanical interaction. Obviously, the higher the linkage between fault segments, the more prone they are to break in cascading coseismic events (Manighetti et al., 2007). Thus, the knowledge of fault interaction is essential to decipher possible future rupture scenarios (Sgambato et al., 2020). Field structural studies focusing on the linkage between adjacent capable faults (e.g., Cowie & Roberts, 2001; Fossen & Rotevatn, 2016; Gupta & Scholz, 2000; Lunn et al., 2008; McClay & Khalil, 1998; Peacock & Sanderson, 1991, 1994; Peacock et al., 2017; Rotevatn & Peacock, 2018; Schlische et al., 1996; Walsh & Watterson, 1991) can help detecting

multisegment sources and assessing the seismogenic potential, based on their cumulative length (Gupta & Scholz, 2000; Iezzi et al., 2020; Peacock & Sanderson, 1991, 1994; Walsh & Watterson, 1991), assuming that this length is comparable to the earthquake maximum coseismic surface rupture length (e.g., Alvarado et al., 2014; Iezzi et al., 2019; Mignan et al., 2015; Nicol et al., 2020; Tondi et al., 2020; Trippetta et al., 2019). The use of empirical relationships linking earthquake rupture size and magnitude (Leonard, 2010; Wells & Coppersmith, 1994) is suggested to assess maximum expected potential magnitude where no compelling data from instrumental, historical, and paleoseismological earthquake catalogs exist. Where possible, these equations should be verified and validated locally as the database on which they are founded usually includes a limited number of events from the studied area and may therefore be poorly applicable. The validation of these empirical equations, together with the assessment of fault segment linkage, is fundamental to better constrain the seismic hazard, particularly where active faults are well-exposed.

The seismically active central Apennines are an excellent natural laboratory for field based studies of active faults. In this study, we focus on the seismic potential of some active normal faults located in the Campo Felice basin (Long. 13°27″E, Lat. 42°13″N, 1,530 m a.s.l.; Figures 1b, 2 and S1), by studying the exposed segmentation and linkage between adjacent fault segments. Italy has a dense seismological network and a rare if not unique historic record of earthquakes (Rovida et al., 2016). The richness of the seismotectonic datasets makes Italy a suitable country to validate the empirical equations between rupture size and earthquake magnitude, using fault length as input data. We apply this approach to the active normal faults of the Campo Felice area (Figures 1, 2 and S1). Although these faults, namely Monte Cefalone (MCF) and Monte Orsello (MOF) faults (Figures 1b, 2, and S1), have not produced documented records of earthquakes in historical times, they are aligned with the seismogenic sources of the L'Aquila 2009 (*Mw* 6.3; e.g., Cheloni et al., 2010) and Avezzano 1915 (*Mw* 7; e.g., Galli et al., 2016) normal fault earthquakes (Figure 1). Moreover, paleoseismological evidence of the occurrence of paleo-earthquakes was documented along these faults (Benedetti et al., 2013; Galli et al., 2008; Giaccio et al., 2003); their geometry and potential mechanical interaction are, however, still unclear.

Based on our and previous geological mapping (Benedetti et al., 2013; Bigi et al., 1995; Ghisetti & Vezzani, 1996; Morewood & Roberts, 2000; Wilkinson et al., 2015), geometric and kinematic analyses (Bigi et al., 1995; Ghisetti & Vezzani, 1996; Morewood & Roberts, 2000; Wilkinson et al., 2015), serial cross-sectioning (Morewood & Roberts, 2000), and throw versus distance diagrams (Benedetti et al., 2013; Morewood & Roberts, 2000; Schlische et al., 1996; Wilkinson et al., 2015) in the Campo Felice area, we evaluated the linkage between fault segments and assessed the seismic potential of the faults in this area. Coupling field observations to Coulomb stress change modeling and employing both known and new empirical relationships between earthquake rupture length and magnitude, we present possible seismic scenarios for the area.

2. Geological Setting

2.1. Central Apennines

The central Apennines are the external domains of a NW-SE-oriented fold-thrust belt that developed since late Oligocene time by the westward subduction of the Adriatic plate below the eastwardly advancing European plate (Carminati & Doglioni, 2012; Dewey et al., 1989; Malinverno & Ryan, 1986). In the analyzed region, Late Miocene – Early Pliocene thrust faulting juxtaposed Lower Jurassic-Middle Miocene carbonates deposited in shallow-water or pelagic environments onto Upper Miocene synorogenic deposits (Cosentino et al., 2010; Ghisetti & Vezzani, 1996; Figure 1b). Since at least Pliocene time, the central Apennines was subjected to NE-SW oriented extension due to the diffuse back-arc stretching affecting the Tyrrhenian side of the orogen (Carminati & Doglioni, 2012; Malinverno & Ryan, 1986). At present, this extensional regime is accommodated by active normal faults striking mainly NW-SE, which have dissected the fold-thrust belt, partly inverting inherited thrust ramps (Cavinato & Celles, 1999; Di Luccio et al., 2010; Tortorici et al., 2019), generating several intermontane basins (e.g., Fucino, Sulmona, Aterno, Campo Imperatore, and Campo Felice basins; Cosentino et al., 2010; Galadini & Galli, 2000; Figure 1b). These active extensional faults generated most of the largest historically and instrumentally recorded earthquakes in central Italy.
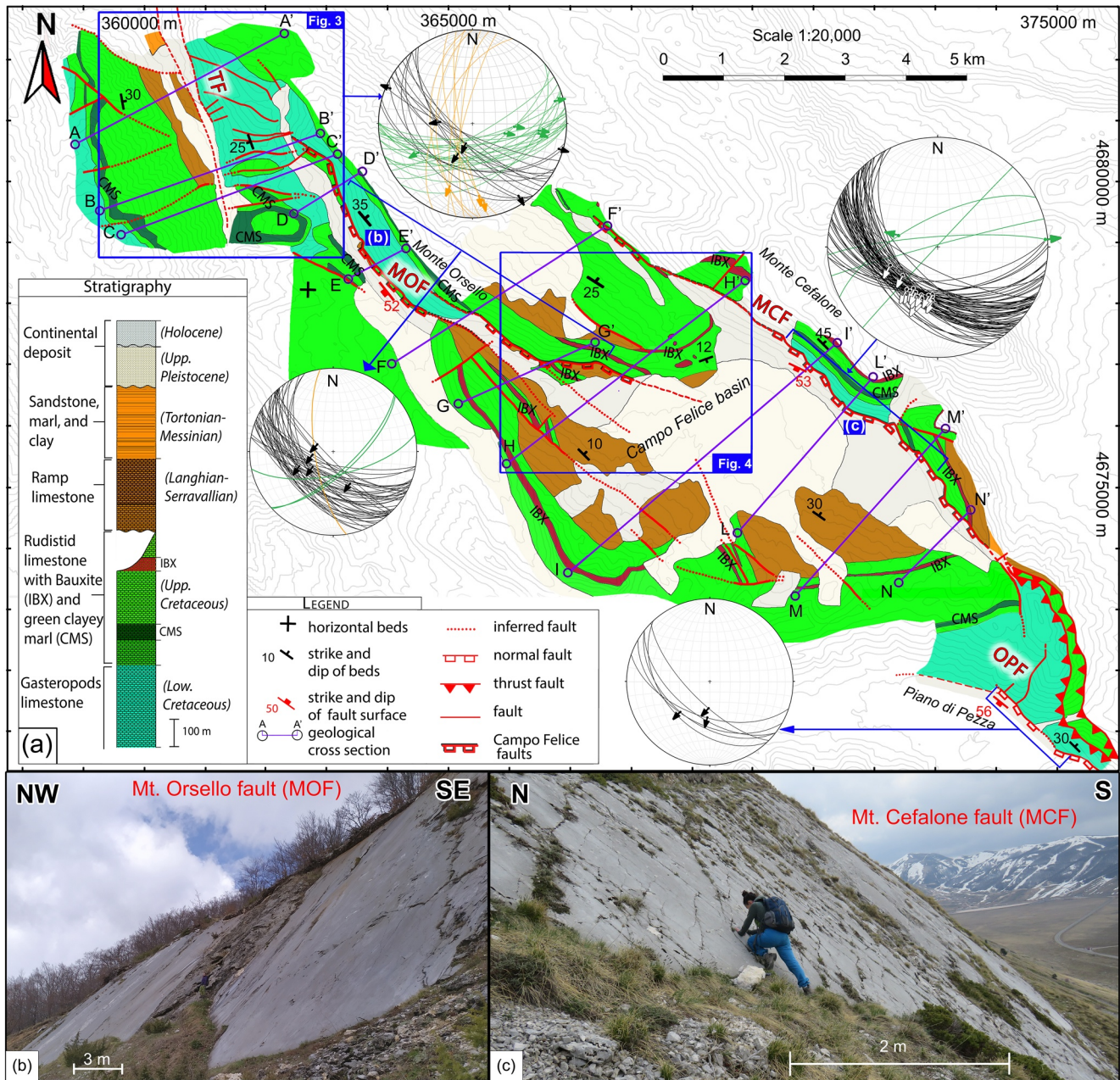
Figure 2. (a) Simplified geological map of the Campo Felice area showing Tornimparte, Monte Orsello (MOF), Monte Cefalone (MCF), and Ovindoli-Pezza faults. This figure includes a simplified stratigraphy of the study area and Schmidt nets (lower hemisphere) showing attitude of fault planes and striae. In the nets, black is for SW-dipping planes, green is for NE-SW-striking planes, and orange is for N-S-striking planes. Tracks of geological cross-sections are in blue (cross-sections are in Figures 5 and S2). Geographic coordinates are based on the UTM system (WGS84- zone 33T). Equidistance between contour lines of topography is 50 m. See Figure S1 for a complete version at the 1:20,000 scale of this map. (b) Outcrop of MOF escarpment (see Figure 2a for its location). (c) Outcrop of MCF fault escarpment (see Figure 2a for its location).

2.2. Campo Felice Basin

The Campo Felice area is a tectonic intermontane extensional basin elongated in a NW-SE direction, filled by alluvial, lacustrine, and glacial deposits (Late Pleistocene to Holocene in age; Giraudi, 1995; Giraudi & Giaccio, 2017; Giraudi et al., 2011; Figures 1b and 2a). The Quaternary basin is surrounded by the Latium-Abruzzi, shallow-water carbonate platform succession (Servizio Geologico d'Italia-APAT, 2006; Figures 1b and 2a), which is capped by the synorogenic Tortonian to Messinian hemipelagic marls and,

in places, by Messinian turbiditic siliciclastic deposits (Brandano, 2017; Cipollari & Cosentino, 1995; Figures 1b and 2a) here named Monte Ocre succession. In particular, in the type-area, Early Cretaceous levels and the unconformable Miocene deposits are widely exposed (Figure 1b). For a detailed description of the Monte Ocre stratigraphic succession, we refer the reader to the supplementary material (Figure S1).

The main evidence of Late Miocene – Early Pliocene contractional tectonics in the Campo Felice area is the Monte Cefalone-Monte Rotondo thrust (e.g., Bigi et al., 1995; Figure 1b). This thrust borders the eastern side of the Monte Cefalone-Monte Serralunga ridge and extends southeastward reaching the Ovindoli and Celano villages (Figure 1b).

The Campo Felice basin is bounded toward the NE by two left-stepping en echelon NW-striking normal faults named Monte Cefalone and Monte Orsello (MCF and MOF, respectively, in Figure 1b), both showing evidence of Late Pleistocene-Holocene activity, documented through geomorphologic and paleoseismological analyses (Benedetti et al., 2013; Galadini & Galli, 2000; Galli et al., 2008; Giaccio et al., 2003; Giraudi, 1995; Giraudi & Giaccio, 2017).

The impressive MCF rock fault scarp (Bosi, 1975) allowed previous authors to infer: (a) through micro-morphologic investigations of the fault surface, the occurrence of two $Mw > 6$ paleoearthquakes, presumably between 860 and 1300 AD, and around 1900 BC, respectively (Giaccio et al., 2003); (b) through ^{36}Cl dating, Holocene slip with at least four exhumation phases, possibly matching earthquakes with $6.2 < Mw < 6.5$, dated back to 9.4, 4.2, 3.4, and 1.1 ka, respectively (Benedetti et al., 2013); (c) through cosmogenic ^{36}Cl concentration, an increase of slip rates in the last 4 ka with a peak between 0.5–2 ka (Goodall et al., 2021).

The MCF pertains to a longer fault system that comprises the Ovindoli-Pezza fault (OPF) to the SE and the Colle Cerasitto fault (CCF) to the NW (Figure 1). The northwestern part of OPF, dipping by 50° toward SW, borders the Piano di Pezza basin with an extensional kinematics (Villani et al., 2015). Here, paleoseismic trenching provided results roughly matching those of MCF, consisting of two $Mw > 6$ events occurred between 860 and 1300 AD, and around 1900 BC, respectively (Pantosti et al., 1996).

The CCF is ~9.5 km long with an average strike of N140° (Salvi et al., 2003). Previous paleoseismological studies on the CCF showed: (a) gravitational displacements in addition to tectonic movements through analysis of COSMO-SkyMed InSAR data (Albano et al., 2015); (b) four shallow faulting events ($6 < Mw < 7$) in the past 20 kyr through GPR investigations (Salvi et al., 2003), three of which roughly matching the radiometric ages obtained for the events along OPF (Pantosti et al., 1996) and MCF (Giaccio et al., 2003). Based on these paleoseismological analyses, OPF, MCF, and CCF possibly ruptured together during some past earthquakes, releasing $Mw \sim 6.7$ events with a recurrence time of ~2.5 ka (Galli, 2020). Alternatively, these faults may have ruptured separately, thus originating earthquakes of lower magnitude (~6.3; Galli, 2020). Paleoseismological studies provide an estimated throw-rate for these faults (MCF, OPF, and CCF) spanning between 0.8 and 1.3 mm/yr during the last 18 ka (Galadini & Galli, 2000; Papanikolaou et al., 2005).

So far, the MOF (Figure 1) has not been studied and mapped in detail. Therefore, its geometrical relationship with the MCF is not completely clear (Bigi et al., 1995; Ghisetti & Vezzani, 1996; Morewood & Roberts, 2000). There are no paleoseismological studies on the MOF, although its eastern prolongation across the Campo Felice basin cuts through local moraines dated ~36 and ~17 ka (Giraudi & Giaccio, 2017; Giraudi et al., 2011). This evidence suggests a late Quaternary activity for MOF as well. Moreover, Tondi and Cello (2003) suggested the MOF to be the seismogenic source of the 1786 L'Aquila earthquake.

To NW of MOF, the presence of the Tornimparte fault (TF), which continues northward for about 7 km, is inferred from the almost rectilinear contact between lower Cretaceous Gastropods limestones and Messinian synorogenic deposits (Servizio Geologico d'Italia-APAT, 2010). The principal surface of the TF is exposed in the northern portion and is characterized by predominant left-lateral strike-slip kinematic indicators (Bigi et al., 1995; Centamore & Dramis, 2010). The lack of faulted Quaternary deposits does not permit any inference regarding its activity under the present and recent NE-SW extensional stress field. Nevertheless, Tondi and Cello (2003) proposed the TF as the seismogenic source of the 1349 L'Aquila earthquake.

3. Methods

3.1. Field Mapping

The purpose of our field structural analysis is investigating the fault geometry and kinematics. During the 1:10,000 field surveys, we (a) focused in particular on the tip areas of the Campo Felice faults (MOF and MCF), and (b) carefully mapped and measured the lateral continuity of the faults to obtain reliable results on the potential surface rupture length. We labeled and mapped "normal faults" and "thrust faults" the structures that we observed directly and measured in the field. With "inferred faults" are labeled structures that we were not able to observe directly in the field but that we deduced through anomalous relationships within the sedimentary succession or whose occurrence we supposed from the prolongation of observed faults. We labeled as "faults" structures directly observed in the field without any kinematic indicator, for which we deduced extensional-oblique kinematics on the basis of the rocks cropping out in the footwall and hangingwall blocks (Figures 2 and S1). For geometric and kinematic analyses of faults and kinematic indicators, we used the lower hemisphere Schmidt stereographic projections. Based on our geological surveys and mapping at the 1:10,000 scale, on the topographic map by CTR Abruzzo (scale 1:10,000), on the geological map and stratigraphy by ISPRA (Foglio 359 "L'Aquila," Servizio Geologico d'Italia-APAT, 2006), and on the digital terrain model with 10 m resolution by CTR Abruzzo, we realized the geological map shown in Figure S1. In detail, we mapped all the faults with trace length >~0.5 km.

3.2. Geological Cross-Sections

The purpose of the construction of 12 serial geological cross-sections at the 1:20,000 scale is the estimation of the vertical component of fault displacements (i.e., fault throws) associated with the studied faults (i.e., TF, MOF, and MCF; Figures 2 and S1). All cross-sections are reported in Figure S2. The cross-section traces are oriented perpendicular to the fault strike, are 1–6 km long, and are spaced about 1 km (Figures 2 and S1). Bedding dip and thickness of formations (Figures 2 and S1) are constrained by our original field data and by previous works (Servizio Geologico d'Italia-APAT, 2004, 2006, and 2010). With the exception of thickness variations in RDT deposits, geological data do not allow us to constrain eventual other thickness variations for Mesozoic and Cenozoic deposits along our geological cross-sections. For this reason, we assumed a constant thickness of these rock units across all cross-sections. Apparent dip of bedding was calculated using the nomogram. To evaluate fault throw, we leveraged on two easily recognizable stratigraphic markers characterized by small thickness and well constrained age. They are the Cenomanian Intra-bauxitic limestones (IBX), with a thickness of ~50 m, and the early Aptian micritic limestones alternating with green clayey marls, with a thickness of ~50 m (Figure S1). In each cross-section, we evaluated the throw of fault segments calculating the difference between elevations of hangingwall and footwall cutoffs with the fault segments.

With the exception of the north-easternmost portion of cross-sections L-L′, M-M′, and N-N′, where boreholes constrain the thickness of Late Pleistocene continental deposits to be 100 m (Giraudi et al., 2011), no geological and geophysical data are available to infer the depth of the bottom of these deposits in the remaining parts of the Campo Felice plain. To avoid over interpretations, we choose to leave blank (with question marks) the contact between the bedrock and continental deposits in the unconstrained areas. Inferred faults below recent deposits are drawn as SW-dipping by 55° and extensional kinematics, coherently with other nearby outcropping faults.

Due to uncertainties/variations of the dip angle of bedding, we attributed an asymmetric error to each throw measurement on fault segments. In particular, we calculated the maximum $(T_i + \delta_{ipos})$ and minimum $(T_i + \delta_{ineg})$ possible throw for each fault segment as follows. T_i is the calculated throw, whereas δ_{ipos} and δ_{ineg} are positive and negative errors, respectively. Even where fault throw was well constrained, we assumed a minimum error of 5 m to take into account possible instrumental uncertainties during measurements with the digital ruler. We also calculated the total throw and its associated error for the main faults (i.e., MCF and MOF). Unconstrained/unrecognized thickness variations of Mesozoic and Cenozoic formations could in principle affect throw calculations. However, since no post-RDT strata were used to calculate the throws, we are confident that the constant thickness assumption does not impact significantly on the evaluation of errors.

Since the throw measurements are independent, we used the method by D'Agostini (2004) to calculate final throw (T_{fin}) and their error (δT) for each main fault:

$$\text{ERROR ANALYSIS} \begin{cases} T_{\text{fin}} = \sum\limits_{i=1}^{n} T_i + \dfrac{\left(\sum_{i=1}^{n} \delta_i^{\text{pos}} + \sum_{i=1}^{n} \delta_i^{\text{neg}} \right)}{2} \\[2ex] \delta T = \dfrac{T_{\text{max}} - T_{\text{min}}}{2} \\[2ex] \text{Where, } T_{\text{max}} = \left(T_1 + \delta_{1\text{pos}} \right) + \left(T_2 + \delta_{2\text{pos}} \right) + \ldots + \left(T_n + \delta_{n\text{pos}} \right) \\[1ex] T_{\text{min}} = \left(T_1 + \delta_{1\text{neg}} \right) + \left(T_2 + \delta_{2\text{neg}} \right) + \ldots + \left(T_n + \delta_{n\text{neg}} \right) \\[1ex] \text{And } 1 \leq i \leq n \text{ is the } i\text{th fault segment in the cross section.} \end{cases}$$

3.3. Fault Distance Versus Throw Diagrams

Fault distance versus throw diagrams were built to investigate the throw distribution along fault strike and to assess the stage of linkage (i.e., soft- vs. hard-linkages; Walsh & Watterson, 1991) between the TF, MOF, and MCF segments. We included in this analysis only the "inferred" fault segments deduced such as prolongation of studied faults. Hard-linkage occurs where fault segments are physically linked by transfer faults (Peacock, 2002). In this case, the fault trace abruptly changes its orientation in map view. Transfer faults linking two faults transmit the total amount of throw from one fault to the other (Boccaletti et al., 1998; Chorowicz & Sorlien, 1992; Moustafa, 2002). In turn, where a soft-linkage occurs, faults are not geometrically linked but they mechanically interact (Gupta & Scholz, 2000; Walsh & Watterson, 1991). In this case, the mechanical interaction between soft-linked faults produces a relay ramp, which is characterized by the reorientation of bedding in fault segment overstep areas to connect the footwall of a fault tip to the hangingwall of the adjacent one (Ferrill & Morris, 2001; Peacock & Sanderson, 1991, 1994; Walsh & Watterson, 1991; Walsh et al., 1999). The evolution from soft-linkage to hard-linkage is characterized by breaching of the relay-ramp, where fractures and faults with horsetail geometry start to link the overstepping segments (Ferrill & Morris, 2001; McClay & Khalil, 1998; Peacock & Sanderson, 1991, 1994). In addition to field observations (i.e., geometry and kinematics of minor faults, and attitude of bedding), diagrams displaying fault displacement versus along strike distance are regularly used to assess the degree of interaction between adjacent fault segments. In such diagrams, the displacement gradient becomes progressively steeper in proximity of soft-linked fault tips: The steeper the gradient, the larger the interaction between faults (e.g., Ferrill & Morris, 2001; Iezzi et al., 2020; Peacock & Sanderson, 1991, 1994; Schlische et al., 1996; Spina et al., 2008; Williams & Chapman, 1983).

3.4. Seismic Potential

The purpose of empirical equations linking rupture size and maximum potential earthquake magnitude is the assessment of the fault seismic potential (i.e., maximum potential earthquake magnitude). We use three empirical equations valid for normal dip-slip faults from Galli et al., (2008), Leonard (2010), and Wells and Coppersmith (1994). Equations by Leonard (2010) and Wells and Coppersmith (1994) are general and used worldwide, whereas the equation by Galli et al. (2008) was specifically developed for the present extensional tectonics of Apennines.

The equation by Wells and Coppersmith (1994) is:

$$Mw = 4.86 + 1.32 \cdot \log \left(L \right) \tag{1}$$

where Mw is the moment magnitude and L is the surface rupture length expressed in km. The standard deviation associated with this equation is 0.34. Equation 1 is empirically based on a worldwide database of 15 selected historical extensional earthquakes and is valid for earthquakes shallower than 40 km with $5.2 < Mw < 7.3$, and for (rupture length) $2.5 < L$ (km) < 41 (Wells & Coppersmith, 1994). The database used by Wells and Coppersmith (1994) mainly includes earthquakes from USA, but it also included five earthquakes from Italy, namely the Avezzano 1915 Mw 7, Umbria 1979 Mw 5.9, Irpinia 1980 Mw 6.9, Lazio-Abruzzo 1984 Mw 5.8, and Umbria 1984 Mw 5.3.

The equation by Galli et al. (2008) is:

$$Mw = 4.7248 * L^{0.1046} \tag{2}$$

where L is the surface rupture fault length expressed in km obtained by mapping of active faults and by paleoseismological studies. This equation is empirically based on a database of 16 paleoearthquakes occurred in the past 2.4 ka in the Apennines with $Mw > 5.5$ (Galli et al., 2008).

The equation by Leonard (2010) is:

$$Mw = 4.40 + 1.52 \cdot \log(L) \tag{3}$$

where L is the surface rupture length expressed in km. Equation 3 is an improvement and refinement of Equation 1. To formulate Equation 3, Leonard (2010) used worldwide databases from previous works (Hanks & Bakun, 2002; Henry & Das, 2001; Manighetti et al., 2007; Romanowicz & Ruff, 2002; Wells & Coppersmith, 1994). Limits of Equation 3 are the same ones of Equation 1.

In order to best estimate the magnitude expected by the faults studied in this work, we compared, through the chi-squared X^2 statistical test (Mann & Wald, 1942), the aforementioned empirical equations (Galli et al., 2008; Leonard, 2010; Wells & Coppersmith, 1994) with data from the last seven $Mw > 5.5$ earthquakes occurred in the central Apennines from 1997 to July 2020 (Table S2). Through linear regression of these seven data, we propose an ad-hoc new empirical equation valid for central Italy that is reported in the Discussion section.

3.5. Coulomb Stress Change Modeling

Coulomb stress change modeling for different earthquakes scenarios was performed to infer post-seismic stress transfer between adjacent fault segments and eventually assess the possibility for a potential cascade or quasi-synchronous activation of adjacent faults during seismic events. We used Coulomb 3.3 software by Toda et al. (2011) and approximated the measured exposed fault length with the coseismic surface rupture length. The width of the rupture (W; i.e., the downdip rupture length) is calculated from the rupture length (L; i.e., the along strike length) using the following equation by Leonard (2010), valid for extensional faults with length >5.5 km:

$$W = 1.7 * L^{0.67} \tag{4}$$

Moreover, the fault bottomset depth (d) is calculated using the rupture width (W; see Equation 4) and the average dip angle of faults (~52°, from field surveys): $d = W \sin 52°$.

Following Okada (1992), we model seismic events on the studied faults with an average coseismic slip (D_{av}) over the total surface of faults. We calculate the average coseismic slip value (D_{av}) using the following empirical equation by Leonard (2010), valid for extensional faults with length >5.5 km:

$$\log(D_{av}) = 0.833 * \log(L) - 1.3 \tag{5}$$

The assumptions of Coulomb stress modeling are as follows: (a) an elastic half-space with uniform isotropic elastic properties is used following Okada (1992); (b) coefficients of pore fluid flow and of static friction are kept constant (Stein et al., 1997); (c) coseismic slip is considered to remain constant along the whole fault (Okada, 1992; Stein et al., 1997); (d) the receiver faults are assumed as not slipping but optimally oriented for seismic failure (King et al., 1994; Lin & Stein, 2004; Stein et al., 1997; Toda et al., 2011).

During an earthquake, Coulomb stress diminishes along the source fault. As this stress cannot simply disappear, it is usually redistributed to other sites along the same fault or to nearby receiver faults. This increase in Coulomb stress could be sufficient to trigger earthquakes at new nearby locations (Stein, 2003). The equation of Coulomb stress change (e.g., Okada, 1992) is defined as:

$$\sigma_c = \tau + \mu * (1 - B) * \sigma_n \tag{6}$$

where σ_c is the Coulomb stress change, τ and σ_n are the changes in shear and normal stress on a given fault plane, $\mu = 0.75$ is the friction coefficient, and $B = 0.47$ is the Skempton's coefficient. Areas with positive Coulomb stress change are more prone to experience future earthquakes, possibly resulting in cascading or quasi-synchronous seismic events. It follows that the wider the lobes of Coulomb stress change, the larger the segment of faults that can seismically slip, and the higher the released magnitude (e.g., King et al., 1994; Okada, 1992).

4. Results

4.1. The Campo Felice Faults

In the Campo Felice area, Mesozoic carbonate beds dip toward NE by about 30° and are crosscut by two segmented main normal faults (MOF and MCF). The study area also includes the southeastern part of TF and northwestern part of OPF (Figure 2). All these main faults are associated with various synthetic, antithetic, or differently oriented subsidiary faults, with 1–10 m throw. MOF and MCF strike NW-SE and dip toward SW by about 50°, are arranged with an en echelon pattern in map view and show corrugations from the metric to kilometric scale (Figures 2 and S1). MOF consists of two ~5 km long overstepping segments that juxtapose Cretaceous limestones on the footwall against Miocene limestones on the hangingwall (Figure 2). MCF is ~9 km long and hosts Cretaceous limestones in the footwall and post Last Glacial Maximum (LGM) deposits in the hangingwall (Figures 2, S1 and S2). Slickenlines and other kinematic indicators on the main fault scarps show dip-slip extensional kinematics (Figure 2). From a kinematic point of view, subsidiary faults can be divided into three main sets: Strike-slip faults striking N-S with high dip angles; oblique-slip faults striking NE-SW with high dip angles; and extensional/oblique slip faults striking NW-SE with intermediate-high dip angles (Figures 2a and 3).

To evaluate the potential linkage with adjacent faults in the field, we carefully analyzed the NW and SE tips of MOF. The area between MOF and TF (Figure 3) is characterized by intensely fractured rocks and abundant secondary faults. Fault planes show patches of cataclasite and fault breccias, suggesting fault activity at different depths. Throws accommodated by subsidiary faults could not be assessed due to the occurrence of heavily damaged rocks and lack of exposed reference horizons, except for the throw (~200 m; Figure 3d) accommodated by the E-striking fault, which is labeled as Accommodation Fault (AF) in Figure 3a. Faults in this zone display a horsetail geometry (Kim et al., 2004; McGrath & Davison, 1995) radiating from the tip of MOF (Figures 3a and S1). In the area between MOF and MCF (Figures 4 and S1), which is characterized by less frequent secondary faults than those observed between MOF and TF (Figures 4a and 4b), bedding is re-oriented from a regional NW-striking NE-dipping attitude to a local NE-striking SE-dipping attitude, hence forming a local relay ramp (Figures 4a and 4c). Unfortunately, between MCF and OPF, only small outcrops of fractured and brecciated bedrocks as well as secondary faults with a few kinematic indicators occur. Such a poor exposure did not allow us to infer the linkage nature between these two faults.

Results from our field surveys and structural analyses of the Campo Felice faults are illustrated in the maps, cross-sections, diagrams, and photographs of Figures 2–5 and S1–S2.

4.2. Throw Versus Distance Diagrams

Cross-sections show domino SW-dipping normal faults across the studied area with bed dip domains toward NE (Figures 5 and S2). The maximum cumulated vertical component of displacements (i.e., throws) are ~880, ~685, and ~1,480 m for TF, MOF, and MCF, respectively (Figure 5 and Table 1). In principle, considering the prevailing strike slip kinematic indicators measured along the TF, the throw measured along this fault could be a geometric artifact associated with out-of-section motion. However, based on its length (~10 km; Servizio Geologico d'Italia-APAT, 2010) an exclusive strike-slip motion cannot produce a vertical throw of 880 m. Moreover, the fact that the average strike of strata at the hangingwall and footwall (i.e., ~N160°; Figures 2a, 3a and S1) parallels the average strike of the studied fault (i.e., ~N165°; Figures 2a, 3a and S1) allows us to exclude this scenario. Similarly, the average strike of bedding at the hangingwall and footwall of MOF and MCF is parallel to faults strike (Figures 2a and S1). This evidence excludes that a significant part of the vertical throw may have been accumulated during previous strike-slip phases.
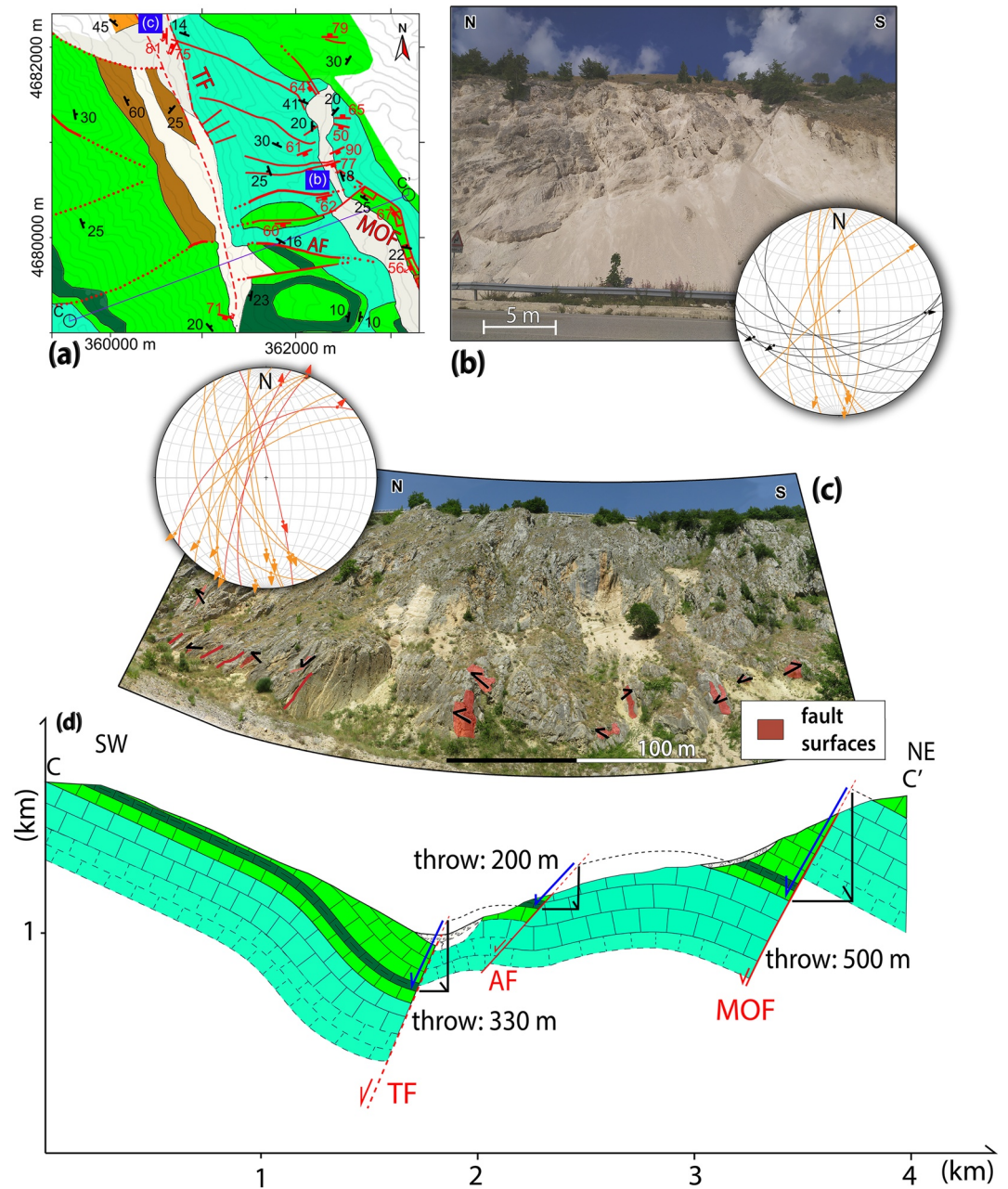
Figure 3. Focus on the area between Tornimparte (TF) and Monte Orsello (MOF) faults (see location in Figure 2a; see also Figures S1 and S2). AF (i.e., Accommodation Fault) indicates a secondary fault with relevant throw, accommodating the throw difference between TF and MOF. (a) Geological map of the area between TF and MOF with track of geological cross-section CC′. For the stratigraphy and legend, refer to Figure 2a. (b) Outcrop of a fault damage zone at the northern termination of MOF (location in Figure 3a). Schmidt net (lower hemisphere) shows, in orange and black, N-S-striking and E-W-striking minor faults, respectively. (c) Outcrop of minor strike-slip faults within the damage zone (location in Figure 3a). Red polygons and black arrows indicate fault surfaces and striae attitude, respectively. Schmidt net (lower hemisphere) shows, in orange and red, left- and right-lateral strike-slip faults, respectively. (d) Geological cross-section CC′, along which we calculated the cumulative throw of TF (∼330 m; Table 1) and MOF (∼500 m; Table 1).
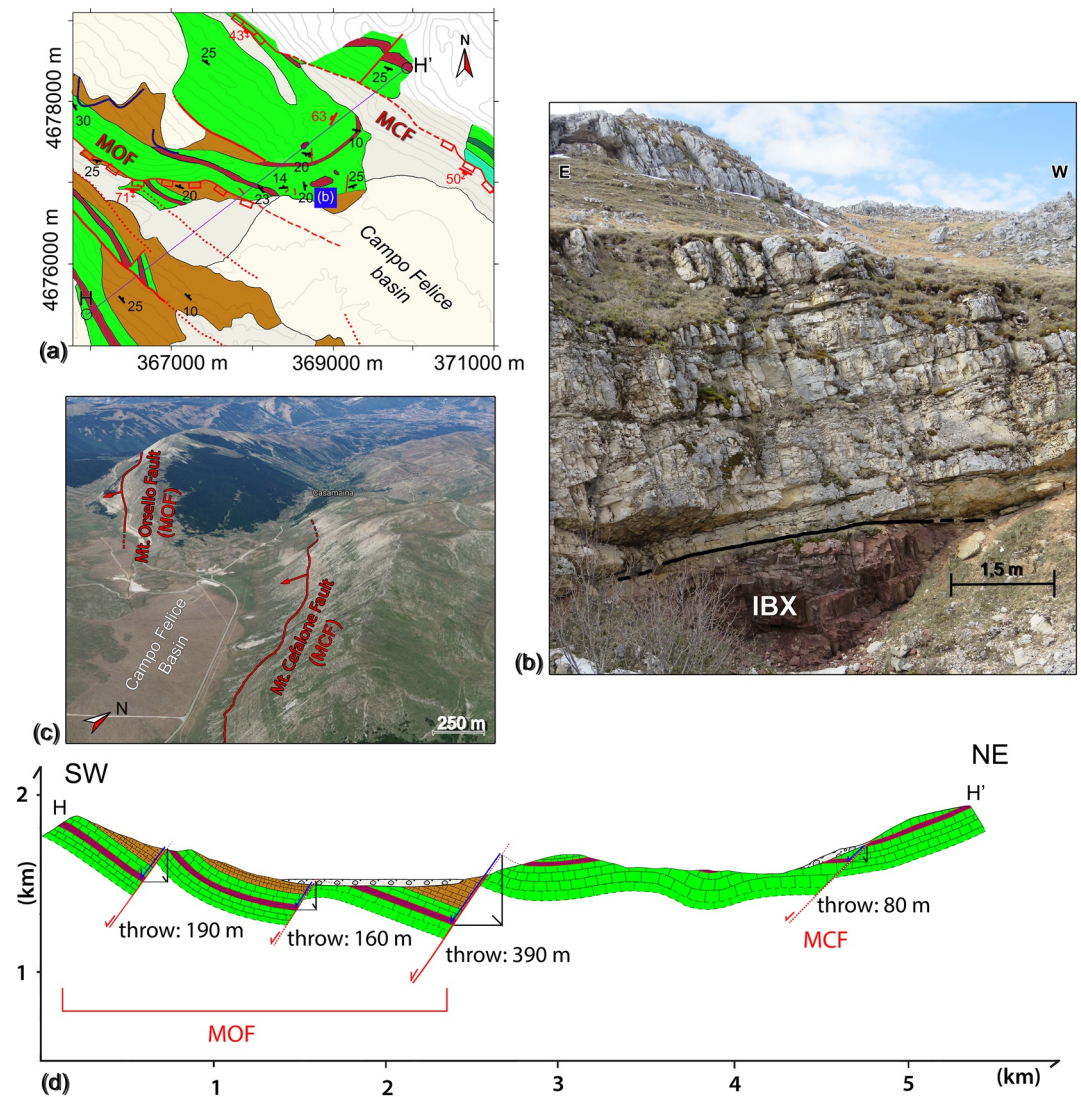
Figure 4. Focus on the area between Monte Orsello (MOF) and Monte Cefalone (MCF) faults (see location in Figure 2a; see also Figures S1 and S2). (a) Geological map with track of geological cross-section HH'. For stratigraphy and legend, the reader is referred to Figure 2a. (b) Outcrop of the stratigraphic boundary between the bauxitic level (IBX) in the bottom and Upper Cretaceous limestones on the top (location in Figure 4a). (c) Satellite lateral view (Google Earth) of the area shown in panel (a). Red lines indicate fault traces. (d) Geological cross-section HH', along which we calculated the cumulative throw of MOF (∼670 m; Table 1) and MCF (∼80 m; Table 1).

In Table 1, we reported all cumulative geological throws and related errors (see the methods section). The throws are plotted against distance along the fault strike in Figure 6. Moving from northwest to southeast, we observe that the TF throw reduces non-linearly toward the fault tip, where the throw gradient is steeper. The throw of MOF has a bell shape typical of most (normal) faults with maximum throw (see cross-sections EE' and GG' in Figure 5) in the central part of the fault, reducing along strike toward the tips, where the gradient is steeper (Figure 6). This is more evident at the southeastern tip than at the opposite tip (Figure 6). It should be considered that the throw reduction (∼200 m) along MOF observed between cross-sections EE' and DD' may have been accommodated by the AF fault (Figure 3), whose eastward continuation is hidden by Quaternary sediments. The throw distribution of MCF has a more pronounced antiformal shape than that observed for MOF, with higher values of throw, which is maximum in the central part of the fault and decreases toward the tips (Figure 6). Approaching the northwestern tip, the throw is very low (<50 m) and the throw gradient is steeper than that observed for the opposite tip (Figure 6).
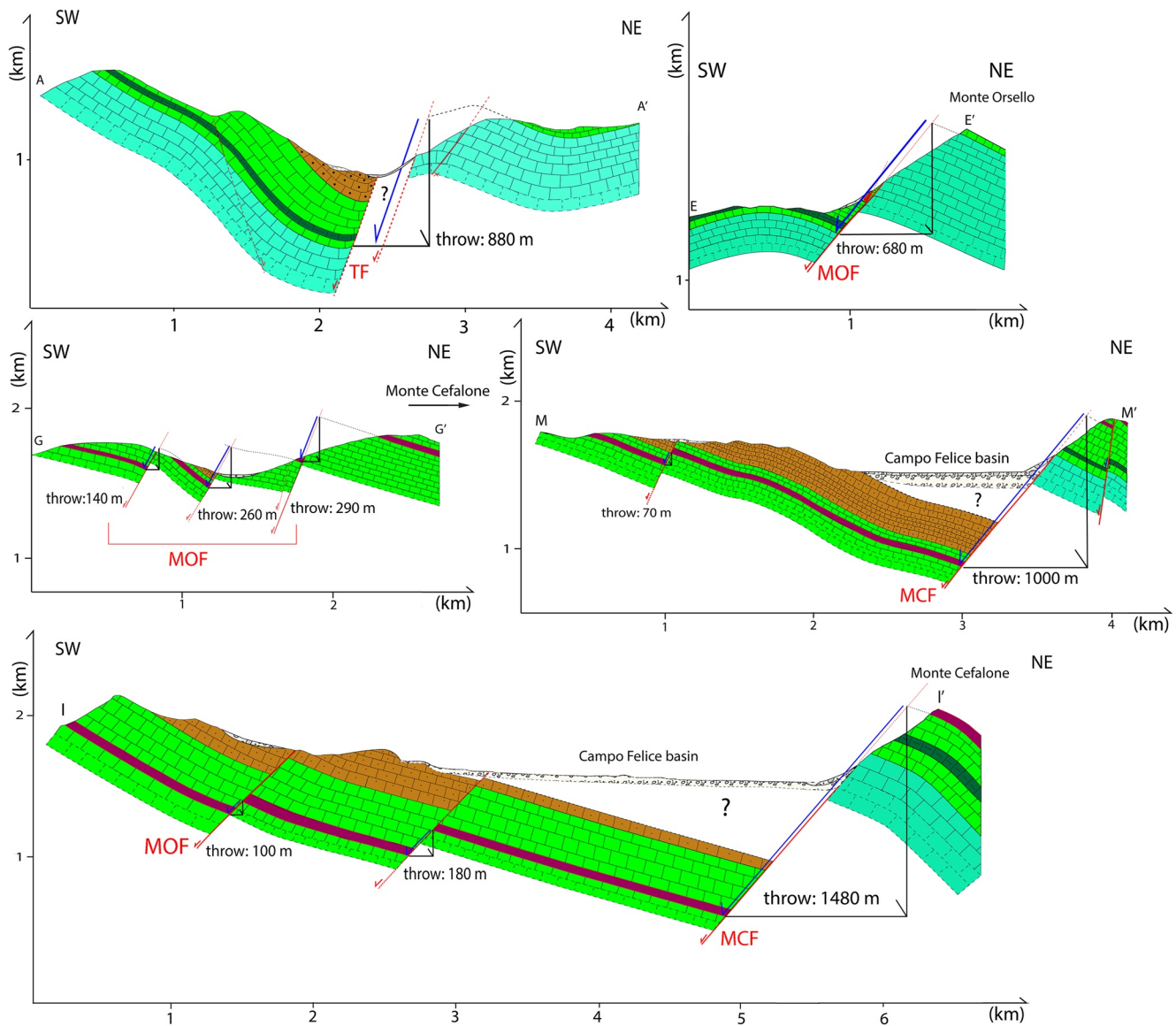
Figure 5. Geological cross-sections AA′, EE′, GG′, II′, and MM′ (see also Figure S2) built across the Tornimparte, Monte Orsello, and Monte Cefalone faults in the Campo Felice area. See Figure 2 for cross-section tracks, stratigraphy, and legend. The color of arrows is: Red for faults, blue for fault displacement, and black for fault throw. The thickness of continental deposits is consistent with Giraudi et al. (2011).

4.3. Seismic Potential

In this section, most of the above-presented data and results are used and synthesized to infer the seismic potential of the Campo Felice normal faults. This is evaluated through empirical relationships between rupture length and earthquake magnitude, assuming that the exposed fault lengths correspond to the maximum future coseismic surface rupture lengths (e.g., Alvarado et al., 2014; Iezzi et al., 2019; Mignan et al., 2015; Nicol et al., 2020; Tondi et al., 2020; Trippetta et al., 2019). We apply Equations 1–3 to our measurements of the exposed Campo Felice fault lengths (MCF and MOF) to obtain the related maximum potential magnitude of earthquakes (Table 2). In particular, we assume both an independent motion of the two studied faults, using the exposed single lengths of MOF and MCF, and a synchronous motion of the two faults, using their cumulative exposed length calculated from the northwestern tip of MOF to the southeastern tip of MCF (Table 2). The resulting magnitude is comprised between *Mw* 5.7 and 6.4 (Table 2). In detail, Equation 1 provides *Mw* values of ~6.0 for MOF, ~6.1 for MCF, and ~6.4 for synchronous motions of MOF and MCF, whereas Equations 2 and 3 provide *Mw* values of ~5.7 for MOF, ~5.9 for MCF, and ~6.2

Table 1
List of Cumulative Fault Throws and Associated Errors, Calculated From Cross-Sections of Figure S2

CROSS-SECTION	TF throw (m)	Error neg (m)	Error pos (m)	MOF throw (m)	Error neg (m)	Error pos (m)	MCF throw (m)	Error neg (m)	Error pos (m)
A	880	−120	50	/	/	/	/	/	/
B	570	−40	330	230	−150	150	/	/	/
C	330	−100	5	500	−150	10	/	/	/
D	/	/	/	460	−75	5	/	/	/
E	/	/	/	680	−40	5	/	/	/
F	/	/	/	540	−50	50	50	−40	150
G	/	/	/	685	−70	70	/	/	/
H	/	/	/	670	−170	170	80	−40	20
I	/	/	/	100	−20	10	1,480	−350	20
L	/	/	/	/	/	/	1,150	−100	40
M	/	/	/	/	/	/	1,000	−50	100
N	/	/	/	/	/	/	450	−80	5

Note. For each value of throw, we associated a confidence interval: Positive error (pos.) defining the possible maximum throw and negative error (neg.) defining the possible minimum throw. TF is Tornimparte Fault, MOF is Monte Orsello Fault, and MCF is Monte Cefalone Fault in Figures 2 and S1.

for synchronous motions of MOF and MCF (Table 2). These seismic potentials are further treated in the discussion section.

4.4. Coulomb Stress Change Modeling

Coulomb stress change modeling was performed to investigate the post-seismic stress transfer between adjacent fault segments. Applying this modeling, we assumed the measured fault length to be equal to the maximum seismic surface rupture length. Geometry (fault length, L, and attitude) and kinematics of faults are retrieved from our field survey. Other input data, such as the downdip rupture length and coseismic average slip (i.e., W and D_{av} in Table 2), were calculated using the well-established empirical Equations 4 and 5 by Leonard (2010). The average coseismic slip (D_{av}) obtained for the studied faults is comprised between 0.3 and 0.5 m (Table 2). These results are consistent with the average slip that occurred during recent earthquakes with rupture lengths of about 10–15 km in the central Apennines (e.g., 0.3 m for the *Mw* 6.0 Colfiorito 1997 by Hunstad et al., 1999; 0.6 m for the *Mw* 6.3 L'Aquila 2009 earthquake by Cheloni et al., 2010; 0.4–0.6 m for the *Mw* 6.5 Norcia 2016 earthquake by Scognamiglio et al., 2018).

We assume a common depth of ∼5 km for the nucleation of earthquakes, consistent with the depth of the hypocenters of recent seismic events in the central Apennines (i.e., depths from 3 to 10 km; Chiaraluce et al., 2003; Cheloni et al., 2010; Galadini et al., 2018).

We performed Coulomb stress change models for both independent and synchronous coseismic slip along MOF and MCF, as summarized in Figure 7, which shows how these ruptures can cause a positive change of Coulomb stress on nearby optimally oriented receiver faults.

The model of coseismic rupture along MOF ($L = 7$ km, $W = 6$ km, and $D_{av} = 0.3$ m; Figure 7a) shows an area with positive Coulomb stress change (∼3 bar) at seismogenic depth on MCF and on the southern part of TF. The coseismic rupture modeled over MCF ($L = 9$ km, $W = 7.5$ km, and $D_{av} = 0.3$ m; Figure 7b) produces a positive Coulomb stress change (∼3 bar) at seismogenic depth over MOF and with minor intensity (∼1 bar), on the northern part of OPF. Finally, modeling synchronous coseismic ruptures along MOF and MCF ($L = 15$ km, $W = 11$ km, $D_{av} = 0.5$ m; Figure 7c), we obtain a positive Coulomb stress change (∼3 bar) at seismogenic depth over the southern part of TF and the northern part of OPF, and with minor intensity (∼1 bar) on CCF.
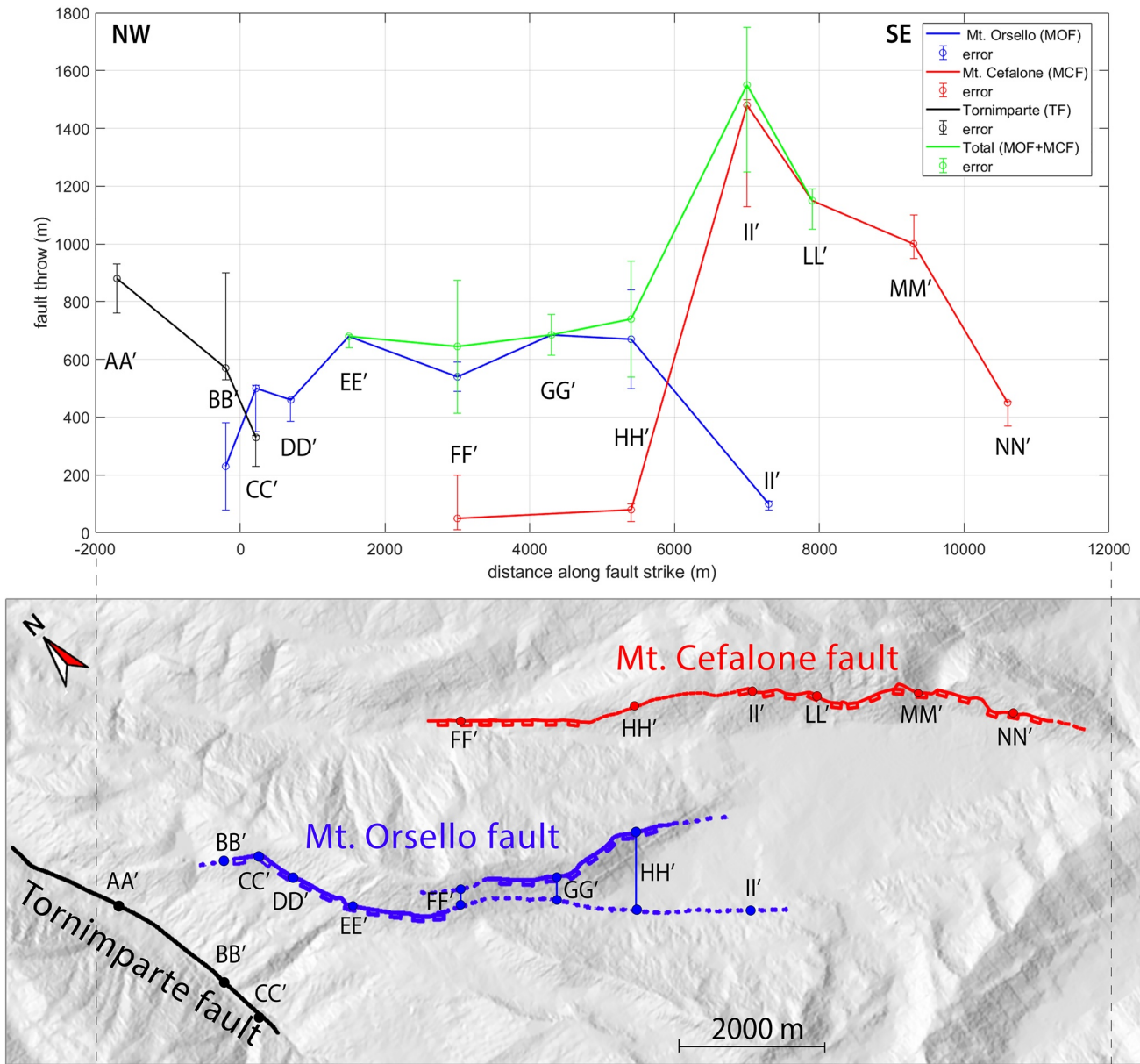
Figure 6. Fault throw profiles along the Tornimparte, Monte Orsello, and Monte Cefalone faults (above) and schematic map of these faults (below). In the map, intersections between cross-sections and faults are indicated with the labels of cross-sections (AA′, BB′, CC′, etc.).

Table 2
List of Fault Lengths (L), Maximum Potential Earthquake Magnitude (Mw) Obtained From Known Empirical Equations 1–3, Compared With the Estimation From the New Equation 7, Discussed Below

Fault name	L (km)	Mw (1)	Mw (2)	Mw (3)	Mw (7)	W (km)	d (km)	D_{av} (m)
Monte Cefalone (MCF)	9	6.12	5.95	5.85	5.90	7.5	6	0.3
Monte Orsello (MOF)	7	5.97	5.79	5.68	5.75	6	5	0.3
Monte Cefalone-Monte Orsello (MCF-MOF)	15	6.41	6.27	6.19	6.22	10.5	8	0.5

Note. Fault width (W) was obtained by using Equation 4, depth of bottomset fault (d) was obtained through W ($d = W \sin 52°$), and average slip (D_{av}) derived from Equation 5.
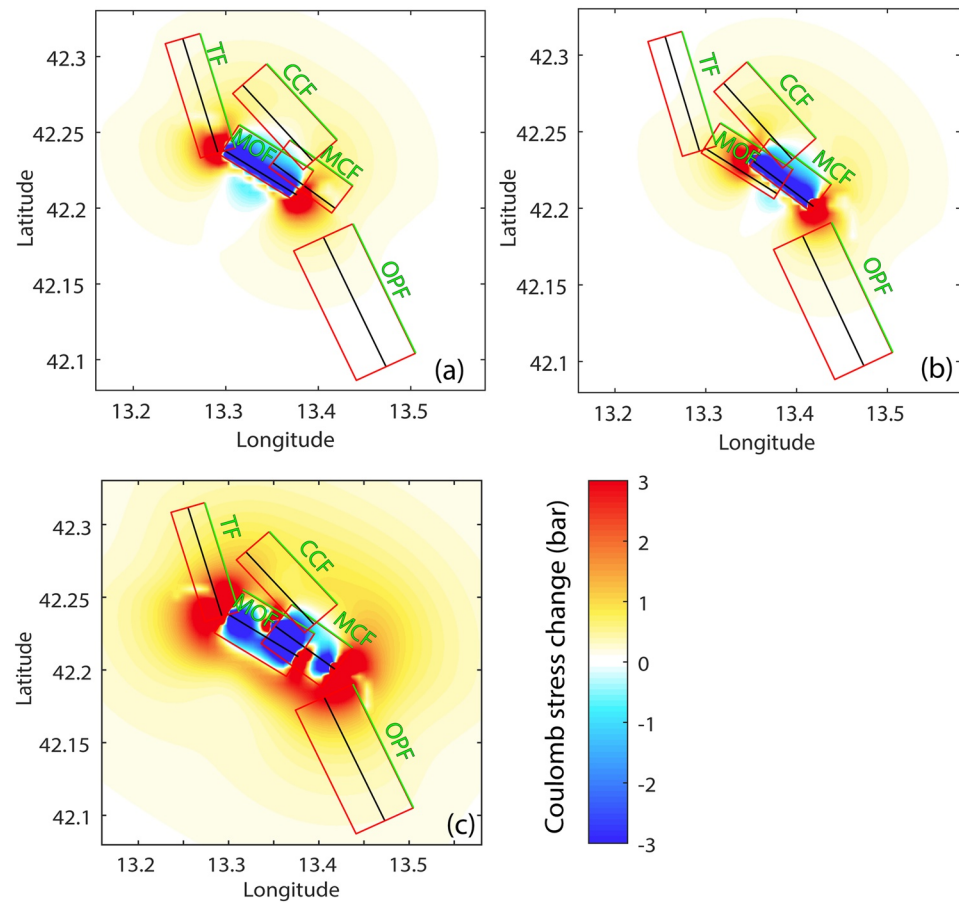
Figure 7. Models of Coulomb stress change induced by supposed earthquakes at ~5 km of depth and with an average coseismic slip on: (a) Monte Orsello fault (MOF) by 0.3 m of slip; (b) Monte Cefalone fault (MCF) by 0.3 m of slip; (c) MOF and MCF simultaneously by 0.5 m of slip (Table 2).

5. Discussion

5.1. Throw Rate

The detailed cumulated throw versus distance diagram of the MCF defines the distribution of the throw accommodated by this fault since its activation (Figure 6). This result can be compared to the post LGM (i.e., post 27–19 ka according to Clarks et al., 2009; post 30–15.5 ka in this area according to Galli et al., 2012) throw distribution measured by Wilkinson et al., (2015) for the southeastern part of the same fault segment (Figure 8). We observed a similar trend that reaches the maximum throw value (more than 1,000 m in our study and 14 m for the post LGM) in the same sector of the fault, with a distribution of throw along the fault strike that persisted almost unchanged through time (Iezzi et al., 2019; Walker et al., 2009). Upon the assumption of post-orogenic development for MCF (i.e., there is no evidence for previous tectonic phases on MCF; Figure 2a), this comparison allows us to infer the onset of the MCF activity (Figure 8). Indeed, by considering the maximum post-LGM throw (about 14 m), we obtain a maximum throw rate of 0.9 mm/yr during the last 16 ka (Wilkinson et al., 2015) for MCF, similarly to many Apennines recent or active faults (Galli & Peronace, 2014). In particular, our evaluation is consistent with Goodall et al. (2021), where the authors assessed a long-term average throw rate for MCF of 1.15 ± 0.36 mm/yr by cosmogenic ^{36}Cl concentration. Assuming a long-term average throw-rate of 0.9 mm/yr for MCF and considering its maximum throw of ~1,400 m (see Figure 6 and cross-section II′ in Figure 5), we obtain that MCF was activated since ~1.5 Ma. This result is consistent with the data published by Giaccio et al. (2012) for the nearby Aterno basin (L'Aquila), formed since about 1.8 Ma. Other studies proposed earlier onset for nearby faults in the study area (Cosentino et al., 2017; Gori et al., 2017; Nocentini et al., 2017). Such an earlier onset is still consistent
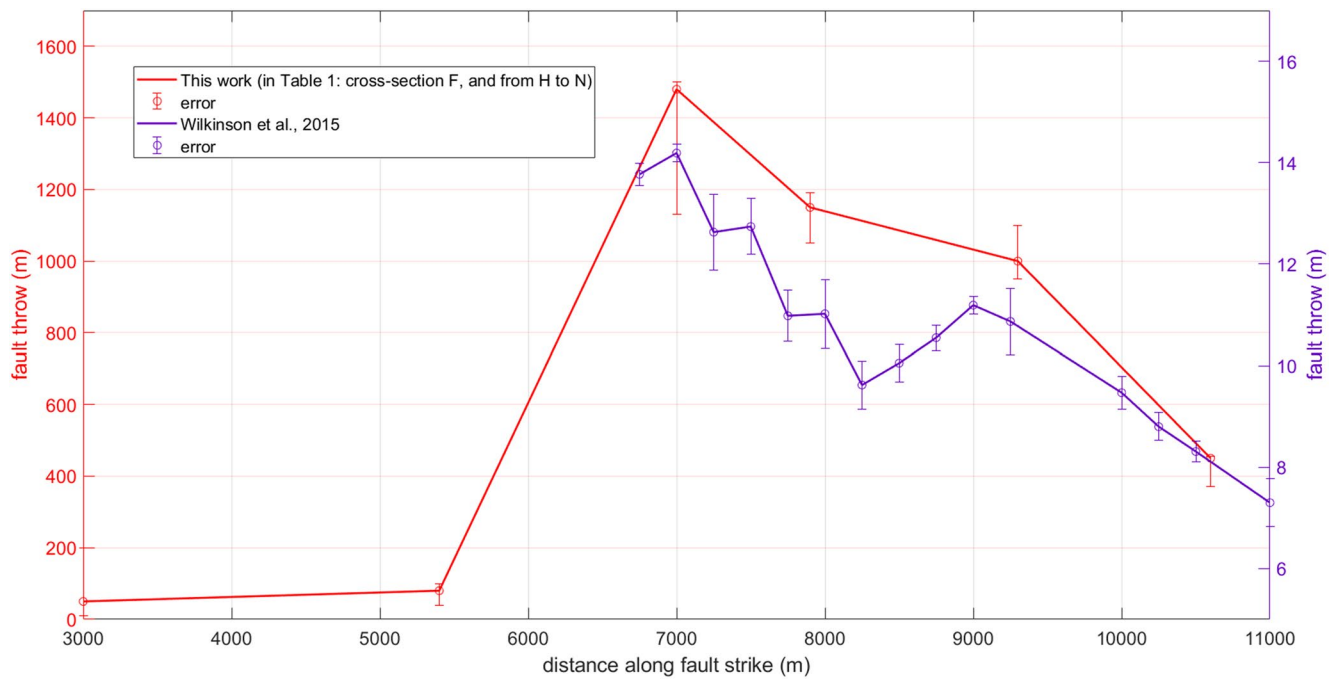
Figure 8. Diagram showing the variation of fault throw with distance along the strike of the southeastern portion of the Monte Cefalone fault (MCF). Red is for cumulative geological (probably younger than 1.5 Ma) throw assessed in this work from cross-sections in Figures 5 and S2 (Table 1), whereas purple is for post LGM (post 16 ka) cumulated throw assessed by Wilkinson et al. (2015) (see Figure 7e of their work) for the same fault (MCF). Left *y*-axis is for post 1.5 Ma throws whereas right *y*-axis is for post 16 ka throws. The two throw datasets and patterns are geologically consistent.

with our inference (about 1.5 Ma for MCF). Note also that our dating calculation (about 1.5 Ma) may be slightly overestimated because the considered throw (∼1,400 m) has a high negative error bar (i.e., −350 m; Figures 6 and 8; Table 1) due to the uncertain thickness of recent deposits of the Campo Felice basin (see question mark beneath the Campo Felice basin in the II′ cross-section in Figure 5).

5.2. Linkage Between Faults

In extensional settings, lateral linkage of faults is an important mechanism controlling fault growth (Peacock, 2002). Growth by linkage produces the increase of length of possible seismic ruptures. Subsequent to a hard linkage, indeed, the segment tips may not act anymore as persistent barriers to seismic ruptures and coseismic slip may therefore propagate from one fault to its neighbor (Manighetti et al., 2007; Moustafa, 2002; Zhang et al., 1991). Moreover, empirical studies have shown that normal faulting earthquakes are capable of rupturing multiple segment barriers that can be up to 5–7 km in length along the fault strike (Iezzi et al., 2019; Wesnousky, 2008). Examples of normal faulting earthquakes that ruptured simultaneously parallel faults spaced about 5 km are the 1954 *Mw* 7.2–6.8 events in Fairview Peak-Dixie Valley (Nevada, USA) and the 1959 *Mw* 7.5 event in Hebgen Lake (Montana, USA) (DePolo et al., 1991).

The evaluation of the stage of linkage between outcropping segments of seismogenic faults can be therefore important to assess future rupture scenarios also at hypocentral depths (Iezzi et al., 2019; Manighetti et al., 2007; Zhang et al., 1991). This can be achieved by integrating field observations (i.e., detailed fault mapping as wells as damage of rocks and kinematic analysis) with the throw versus distance diagrams shown, for instance, in Figure 6 (e.g., Moustafa, 2002; Spina et al., 2008, 2009; Trudgill & Cartwright, 1994). We applied this approach to the studied normal Campo Felice faults (Figure 2).

MOF and MCF (Figure 2a) are characterized by pure dip-slip kinematics on SW-dipping main fault segments, coherently with both the present-day NE-SW oriented sub-horizontal minimum principal stress (e.g., Anzidei et al., 2009; D'Agostino et al., 2001; Devoti et al., 2010; Doglioni et al., 2015; Montone et al., 2004) and the focal mechanisms of recent earthquakes (e.g., Scognamiglio et al., 2010). In the relay zone between

MOF and MCF, we observed only the presence of short faults (length < 100 m in map view, Figure 4a). In this area, a re-orientation of bedding occurs, defining a relay ramp (Figures 4a and 4c). The throw versus distance diagram is characterized by a maximum in the central part of both faults, with the throw decreasing moving along strike toward the fault tips (Figure 6). In Figure 6, we also observed different maximum throws accumulated by the Campo Felice faults. In particular, the cumulative throw of MCF is larger than that of MOF (although part of this difference could be due to the large negative error bar associated with the MCF datum). This is probably due to the fact that MCF, besides being longer than MOF, became active before MOF. The late linkage and common slip with MOF can explain and justify the different throw. Unfortunately, available geological data do not allow the recognition of Holocene or Pleistocene stratigraphic markers nearby the Campo Felice faults, so to reconstruct in detail their throw evolution. New geophysical or subsurface geological data are needed to unravel this issue. In conclusion, both the steep throw gradient of MOF and MCF in their overstepping zone and the increase of their cumulative throw in the same area (Figure 6) point to a linkage between these faults (Ferrill & Morris, 2001; Peacock & Sanderson, 1991, 1994; Walsh & Watterson, 1991; Walsh et al., 1999). It is worth noting that the mechanical and geometrical interaction between fault segments observed in the field do not necessarily reflect the interaction between segments at seismogenic depths. Indeed, different evolutionary stages (from soft-linkage accommodated by relay ramp to hard-linkage accommodated by transfer faults) can develop through time and space, including depth (Fossen & Rotevatn, 2016; Peacock & Sanderson, 1994). A common observation is that the linkage increases with depth (e.g., Fossen & Rotevatn, 2016). Therefore, due to the assessed surface-shallow soft linkage between MOF and MCF, a hard-linkage between MOF and MCF is very likely to occur at seismogenic depth, forming a single seismogenic fault segment (e.g., Spina et al., 2008; Wesnousky, 2008). Based on this mechanical interaction between MOF and MCF and the extensional kinematic indicators measured along these faults (coherent with present-day tectonic setting; Figure 2), we will evaluate seismic potential and seismic scenarios for the Campo Felice area, assuming both an independent and a synchronous future activation of these two faults (Figure 7 and Table 2).

We have also investigated the northwestern tip of MOF (Figures 2 and 3) to understand its possible role during an earthquake. In this area, a ~1.5-km left lateral step with the TF occurs. In the overlapping area, minor faults occur, showing a horsetail like geometry in map view, various orientations, and both dip- and strike-slip kinematics (Figure 3). The oblique slip on NE-SW-striking faults is coherent with the present NE-SW-oriented extension in the Apennines and with dip-slip kinematics on the main active SW-dipping faults. Conversely, oblique slip on SW-dipping faults and strike-slip kinematics on N-S-striking faults are poorly or not coherent with the present tectonic regime. Since there is no clear and systematic evidence of cross-cutting or abutting relationships between the different fault sets, an alternative explanation for this complex kinematics other than a pre-Late-Pliocene motion is the local re-orientation of stress field occurring at fault tips (Fossen & Rotevatn, 2016; Peacock & Sanderson, 1994). The very steep throw gradient of MOF and TF near their overstepping tips (Figure 6), the well-oriented strike of the TF in the present stress field, and the occurrence of minor faults with horsetail geometry linking MOF and TF suggest a shallow-surface soft-linkage with a breached relay-ramp between these faults. In this scenario, the AF fault may have transferred part of the throw (~200 m; Figure 3d) from MOF to TF (Ferrill & Morris, 2001; McClay & Khalil, 1998; Peacock & Sanderson, 1991, 1994). The reactivation of previous strike-slip faults as extensional faults is long known in the Apennines (Cello et al., 1997; Pace et al., 2002; Tondi & Cello, 2003). In such a context, the heavily fractured/damaged rocks at the northwestern tip of MOF can be explained not only with a tip damage zone (Kim et al., 2004; Peacock et al., 2017), but also with a strike-slip to extensional reactivation with fast dynamic shear propagation of coseismic rupture (Reches & Dewers, 2005) toward the TF. Unfortunately, due to its bad exposure, no paleoseismological studies were performed on the TF to exclude or support its reactivation as an extensional fault. Consequently, we will not assume the activation of TF in our models of future coseismic scenarios. Further studies are required to shed light on the role in the past and possibly in the future of the TF.

5.3. A New Magnitude-Length Empirical Equation

We previously used empirical equations from the literature (Table 2) to assess the seismic potential of Campo Felice faults. To understand which of these equations are the best for the central Apennines and Campo Felice area, we compared the magnitude deduced from seismic analyses with that predicted by
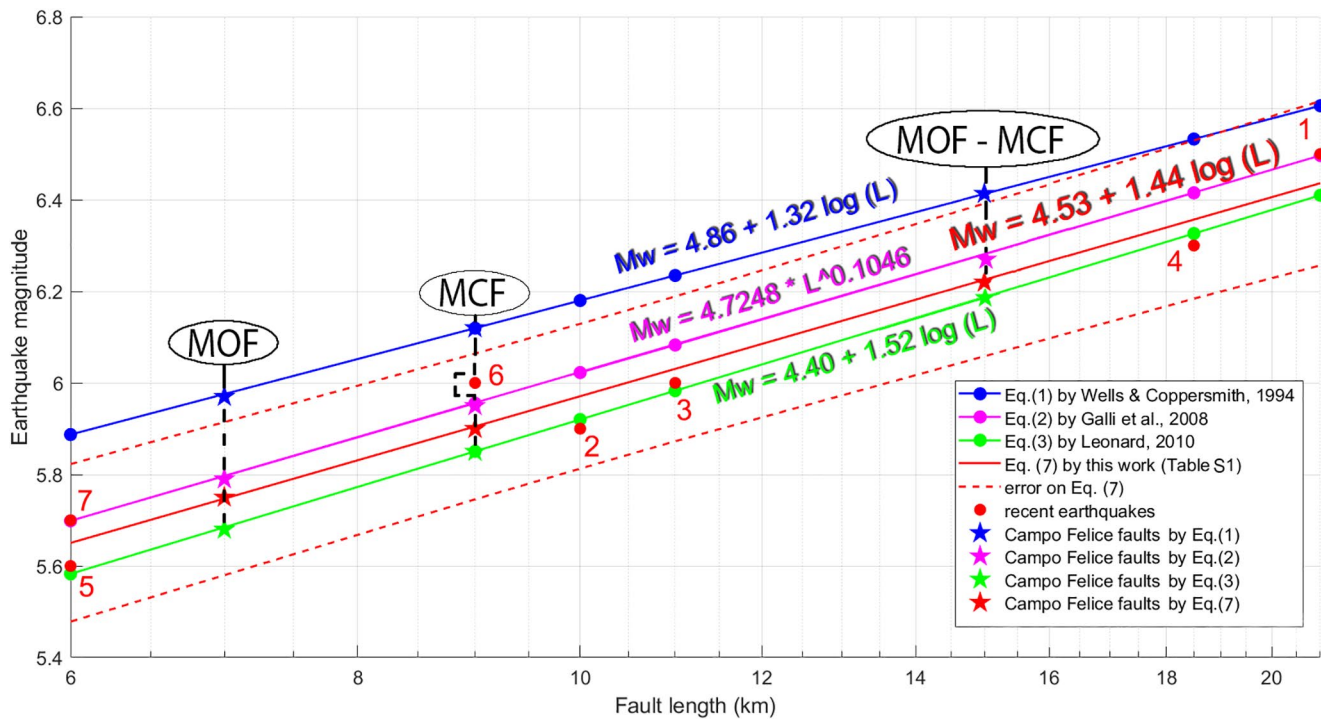
Figure 9. Empirical equations used in this work to calculate the potential maximum moment magnitude (*Mw*) from exposed lengths (*L*) of Monte Orsello (MOF) and Monte Cefalone (MCF) faults as well as from the two faults together (see Table 2). Blue line is for Equation 1 by Wells and Coppersmith (1994), pink line is for Equation 2 by Galli et al. (2008), green line is for Equation 3 by Leonard (2010), and red line is for our new Equation 7 with standard deviation of 0.16 (dotted red lines). Stars are *Mw* assessed with Equations 1, 2, 3, and 7 from the exposed length of MOF, MCF, and their sum. Red dots are the last recent seven earthquakes that occurred in central Apennines with *Mw* > 5.5, namely the 2016 Norcia *Mw* 6.5, 2016 Visso *Mw* 5.9, 2016 Amatrice *Mw* 6.0, 2009 L'Aquila *Mw* 6.3, 1997 Colfiorito *Mw* 5.6, 1997 Colfiorito *Mw* 6, and 1997 Colfiorito *Mw* 5.7 earthquakes (Table S1).

Equations 1–3 for the last seven *Mw* > 5.5 earthquakes (1997–2016) from the central Apennines (Figure 9; Table S1). These earthquakes (Figure 1a) are: Colfiorito, September 26, 1997 (*Mw* 5.7 and 6; Chiaraluce et al., 2003), Sellano, October 14, 1997 (*Mw* 5.6; Chiaraluce et al., 2003), L'Aquila, April 6, 2009 (*Mw* 6.3; Guerrieri et al., 2010), Amatrice, August 24, 2016 (*Mw* 6.0; Galadini et al., 2018), Visso, October 26, 2016 (*Mw* 5.9; Galadini et al., 2018), and Norcia, October 30, 2016 (*Mw* 6.5; Galadini et al., 2018).

Although *L* used in Equations 1–3 is the surface rupture length, the subsurface rupture lengths for the last seven *Mw* > 5.5 central Apennines earthquakes as obtained by inverting different types of datasets from previous literature (e.g., earthquake locations from Chiaraluce et al., 2003, InSAR from Galadini et al., 2018 and Guerrieri et al., 2010, and GPS data from Galadini et al., 2018; Table S2). The use of subsurface rupture lengths inferred from geodetic and geophysical interpretations for recent earthquakes in central Apennine is compelled by the fact that coseismic surface ruptures, strongly controlled by rock rheology (Carminati et al., 2020; Tondi et al., 2020), were not continuous in the field (Basili et al., 1998; EMERGEO Working Group, 2010; Falcucci et al., 2018; Pucci et al., 2017). However, in our view, rupture lengths constrained using geophysical data are best comparable with total lengths of exhumed faults, which are the results of tens to thousands of events. In addition, Trippetta et al. (2019) showed that the difference between evaluations of *Mw* obtained by using empirical equations for surface rupture lengths and for subsurface rupture lengths of Leonard (2010) and Wells and Coppersmith (1994) is less than 5% for major faults (with length > 10 km and earthquake *Mw* ≥ 5). This difference increases to about 15% for smaller faults (i.e., for fault length ≤ 2 km), corresponding to earthquake *Mw* less than about 4.8. Therefore, the difference in maximum potential *Mw* obtained by the empirical equations of Leonard (2010) and Wells and Coppersmith (1994) using surface and subsurface rupture lengths can be often negligible (Trippetta et al., 2019).

The chi-squared X^2 statistical test (Mann & Wald, 1942; Table S2) shows that Equation 1, except for the case of the *Mw* 6.5 Norcia 2016 earthquake (see 1 in Figure 9), tends to overestimate recent instrumental

data (X^2 = 0.14%), whereas Equations 2 and 3 (X^2 = 96% and X^2 = 95%, respectively) mirror the data trend. Consequently, we recommend the use of Equations 2 and 3 to assess the seismic potential of active faults in the Apennines area for $5.5 < Mw \leq 6.5$ and for rupture lengths between about 6 and 21 km (Figure 9).

In addition, we used the aforementioned last seven $Mw > 5.5$ earthquakes from the central Apennines to build a new ad-hoc empirical equation (red line in Figure 9). The obtained empirical equation, characterized by a standard deviation of 0.16, is:

$$Mw = 4.53 + 1.44 \cdot \log(L) \tag{7}$$

where L is the subsurface rupture length.

Using Equation 7, we obtain Mw values of ~5.9 for MOF, ~5.8 for MCF, and ~6.2 assuming synchronous motions of MOF and MCF (Table 2). These values are consistent with those calculated with Equations 2 and 3 (e.g., Galli et al., 2008 proposed an expected earthquake magnitude of ~6.3 for MOF + MCF), but underestimate those (Mw 6.2 and Mw 6.5 for segments of MCF) inferred for paleoearthquakes by Benedetti et al. (2013) probably because the authors did not consider the post-seismic erosion of fault surface (Goodall et al., 2021; Kastelic et al., 2017). Moreover, the magnitudes proposed by Benedetti et al. (2013) were obtained measuring coseismic slip through ^{36}Cl concentrations in limestones forming the MCF fault scarp (see also Schlagenhauf et al., 2011) and as pointed out by the authors themselves, the ^{36}Cl method can slightly overestimate the seismic potential because single coseismic slips under about a 100 years' time interval cannot be resolved.

5.4. Possible Seismic Scenarios

We use Coulomb stress change models to verify whether coseismic slip on the investigated faults could induce a quasi-synchronous or cascade break on adjacent fault segments, thus increasing the released energy and raising regional shaking, damage, and casualties.

The maximum Coulomb stress change predicted by our modeling is ~3 bar (Figure 7). This is coherent with previous real instances in the central Apennines. For example, several aftershocks of the L'Aquila 2009 seismic sequence (central Italy) occurred where the mainshock increased the Coulomb stress by 1 bar (Falcucci et al., 2011). During the seismic sequence of Amatrice 2016 (central Italy), the event of Visso (Mw = 5.9) and Norcia (Mw = 6.5) occurred where the previous Mw 6.0 Amatrice earthquake had caused a Coulomb stress increase of 0.35 and 2–3 bar, respectively (Galderisi & Galli, 2020; Tung & Masterlark, 2018). In addition to the case of the central Apennines, during the 1992 Landers (California, USA) seismic sequence, aftershocks mostly occurred where Coulomb stress had been increased by 0.5–1 bar due to the mainshock (King et al., 1994). Moreover, the largest aftershock occurred close to the area where the highest Coulomb stress increase had occurred (3 bar). During the 2016 Kaikoura (New Zealand) seismic sequence, the progressive seismic rupture evolved where the Coulomb stress had been increased by about 2 bar (Xu et al., 2018).

Based on our Coulomb stress modeling, we suggest that a singular coseismic rupture on MOF (Figure 7a) or MCF (Figure 7b) can trigger MCF or MOF, respectively. Moreover, owing to the potential hard-linkage at seismogenic depth between these two faults, we also modeled the synchronous rupture of MOF and MCF (Figure 7c), which resulted in a positive stress change on OPF and TF. Consequently, even if there is no evidence in the literature for a Quaternary activity of TF, Figure 7 shows that this fault could be loaded and hence potentially activated by synchronous seismic slip on MOF and MCF.

In previous studies (Galadini & Galli, 2000; Galli et al., 2008; Giraudi, 1995; Pantosti et al., 1996; Salvi et al., 2003), the MCF fault was considered as a part of the ~35 km long NW-trending OPF – CCF fault system, which possibly generated earthquakes with Mw as high as 6.7 (Galli, 2020). Our modeling results (Figure 7b) highlight another potential scenario, since an earthquake along MCF could activate MOF or OPF more likely than CCF. However, being CCF very close to MCF (about 2 km), we believe that dynamic stress loading (i.e., the stress increases due to the passage of seismic waves; e.g., Freed, 2005; Kanamori & Brodsky, 2004) from an earthquake on MCF could activate CCF too. In summary, an earthquake (coseismic slip ≥ 0.3 m) over MCF could trigger OPF and CCF, as previously proposed (Galli et al., 2008; Pantosti

et al., 1996; Salvi et al., 2003), but also MOF and (eventually) TF, as shown in this work (Figure 7). Similar processes (i.e., single or multisegment fault activations) were proposed for the nearby Norcia Fault (Galli et al., 2020). In particular, their research showed that the Norcia Fault could be seismically activated not only in conjunction with the Monte Vettore Fault, but also with the Cascia and Monte Alvagnano Faults.

6. Conclusions

In the last 25 years, central Apennines faults caused hundreds of victims during $Mw \geq 6.0$ earthquakes, making their geological investigation and seismic potential evaluation primary goals for the scientific community. We focused our studies on the two Campo Felice faults, which are aligned between other seismogenic sources of the central Apennines and may represent a hitherto silent seismic connection between the catastrophic 1915, Mw 7 Avezzano and the destructive 2009, Mw 6.3 L'Aquila earthquakes (Figure 1). Results of our field surveys, geological-structural mapping, serial cross-sections, and throw versus distance diagrams highlight a shallow soft linkage between the two Campo Felice faults. Based on this mechanical interaction, we evaluate the maximum potential magnitude (Mw) of ~5.8 and 6.2 assuming, respectively, an independent or synchronous activation of these faults. Furthermore, our Coulomb stress change modeling shows that these magnitude assessments could potentially increase considering a quasi-synchronous or cascade activation of the Campo Felice faults together with other conterminous faults. This study shows that, in addition to paleoseismological analyses as well as geophysical investigations, geological mapping and field structural analysis provide significant evidence to draw future seismic scenarios aimed at mitigating the earthquake threat. We emphasize two main conclusions: (a) The degree of linkage between adjacent segments of faults can be assessed through field studies and geological cross-sectioning, where this potential linkage becomes fundamental to correctly assess the seismic potential of fault systems; (b) empirical relationships between fault size and earthquake magnitude are a powerful tool to assess the seismic potential of faults and fault systems, but these relationships should be tested, where possible, against recent local earthquake data. Concerning this latter point, for the central Apennines, the empirical relationships by Galli et al. (2008) and Leonard (2010) and this work (Equation 7) appear as the most reliable and therefore, we recommend their use to estimate the seismic potential of active faults.

Data Availability Statement

All data needed to evaluate the conclusions in the study are present in the supporting information. These data are also freely available in the Figshare external repository (https://doi.org/10.6084/m9.figshare.12102549. v5). Moreover, part of the data used to construct the diagram of Figure 7 (i.e., purple data in Figure 7) are available in Wilkinson et al. (2015).

References

Albano, M., Barba, S., Saroli, M., Moro, M., Malvarosa, F., Costantini, M., et al. (2015). Gravity-driven postseismic deformation following the Mw 6.3 2009 L'Aquila (Italy) earthquake. *Scientific Reports*, *5*, 16558. https://doi.org/10.1038/srep16558

Alvarado, A., Audin, L., Nocquet, J. M., Lagreulet, S., Segovia, M., Font, Y., et al.(2014). Active tectonics in Quito, Ecuador, assessed by geomorphological studies, GPS data, and crustal seismicity. *Tectonics*, *33*(2), 67–83. https://doi.org/10.1002/2012TC003224

Anzidei, M., Boschi, E., Cannelli, V., Devoti, R., Esposito, A., Galvani, A., et al. (2009). Coseismic deformation of the destructive April 6, 2009 L'Aquila earthquake (central Italy) from GPS data. *Geophysical Research Letters*, *36*(17). https://doi.org/10.1029/2009GL039145

Basili, R., Bosi, V., Galadini, F., Galli, P., Meghraoui, M., Messina, P., et al. (1998). The Colfiorito earthquake sequence of September–October 1997: Surface breaks and seismotectonic implications for the central Apennines (Italy). *Journal of Earthquake Engineering*, *2*(02), 291–302. https://doi.org/10.1080/13632469809350323

Benedetti, L., Manighetti, I., Gaudemer, Y., Finkel, R., Malavieille, J., Pou, K., et al. (2013). Earthquake synchrony and clustering on Fucino faults (Central Italy) as revealed from in situ 36Cl exposure dating. *Journal of Geophysical Research: Solid Earth*, *118*(9), 4948–4974. https://doi.org/10.1002/jgrb.50299

Bigi, S., Capotorti, F., Centamore, E., & Fumanti, F. (1995). Caratteri geologico-strutturali dell'area compresa tra Tornimparte ed i Monti d'Ocre (Appennino centrale, Italia). In *Studi geologici camerti, n. speciale* (pp. 87–94). https://doi.org/10.15165/studgeocam-921

Boccaletti, M., Bonini, M., Mazzuoli, R., Abebe, B., Piccardi, L., & Tortorici, L. (1998). Quaternary oblique extensional tectonics in the Ethiopian Rift (Horn of Africa). *Tectonophysics*, *287*(1–4), 97–116. https://doi.org/10.1016/S0040-1951(98)80063-2

Bosi, C. (1975). Osservazioni preliminari su faglie probabilmente attive nell'Appennino centrale. *Bollettino della Societa Geologica Italiana*, *94*, 827–859. Retrieved from http://pascalfrancis.inist.fr/vibad/index.php?action=getRecordDetail&idt=PASCALGEODEBRGM7720198189

Brandano, M. (2017). Unraveling the origin of a Paleogene unconformity in the Latium-Abruzzi carbonate succession: A shaved platform. *Palaeogeography, Palaeoclimatology, Palaeoecology*, *485*, 687–696. https://doi.org/10.1016/j.palaeo.2017.07.025

Brozzetti, F., Boncio, P., Cirillo, D., Ferrarini, F., de Nardis, R., Testa, A., et al. (2019). High-resolution field mapping and analysis of the August–October 2016 coseismic surface faulting (central Italy earthquakes): Slip distribution, parameterization, and comparison with global earthquakes. *Tectonics*, *38*, 417–439. https://doi.org/10.1029/2018TC005305

Carminati, E., Bignami, C., Doglioni, C., & Smeraglia, L. (2020). Lithological control on multiple surface ruptures during the 2016–2017 Amatrice-Norcia seismic sequence. *Journal of Geodynamics*, *134*, 101676. https://doi.org/10.1016/j.jog.2019.101676

Carminati, E., & Doglioni, C. (2012). Alps vs. Apennines: The paradigm of a tectonically asymmetric Earth. *Earth-Science Reviews*, *112*(1–2), 67–96. https://doi.org/10.1016/j.earscirev.2012.02.004

Cavinato, G. P., & Celles, P. D. (1999). Extensional basins in the tectonically bimodal central Apennines fold-thrust belt, Italy: Response to corner flow above a subducting slab in retrograde motion. *Geology*, *27*(10), 955–958. https://doi.org/10.1130/0091-7613(1999)027<0955:EBITTB>2.3.CO;2

Cello, G., Mazzoli, S., Tondi, E., & Turco, E. (1997). Active tectonics in the central Apennines and possible implications for seismic hazard analysis in peninsular Italy. *Tectonophysics*, *272*(1), 43–68. https://doi.org/10.1016/S0040-1951(96)00275-2

Centamore, E., & Dramis, F. (2010). *Note Illustrative Della Carta Geologica d'Italia Alla Scala 1: 50.000, Foglio 358-Pescorocchiano* (Vol. 147). ISPRA-Servizio Geologico d'Italia. Retrieved from http://www.isprambiente.gov.it/Media/carg/note_illustrative/358_Pescorocchiano.pdf

Cheloni, D., D'agostino, N., D'anastasio, E., Avallone, A., Mantenuto, S., Giuliani, R., et al. (2010). Coseismic and initial post-seismic slip of the 2009 M w 6.3 L'Aquila earthquake, Italy, from GPS measurements. *Geophysical Journal International*, *181*(3), 1539–1546. https://doi.org/10.1111/j.1365-246X.2010.04584.x

Chiaraluce, L., Di Stefano, R., Tinti, E., Scognamiglio, L., Michele, M., Casarotti, E., et al. (2017). The 2016 central Italy seismic sequence: A first look at the mainshocks, aftershocks, and source models. *Seismological Research Letters*, *88*(3), 757–771. https://doi.org/10.1785/0220160221

Chiaraluce, L., Ellsworth, W. L., Chiarabba, C., & Cocco, M. (2003). Imaging the complexity of an active normal fault system: The 1997 Colfiorito (central Italy) case study. *Journal of Geophysical Research*, *108*(B6). https://doi.org/10.1029/2002JB002166

Chiaraluce, L., Valoroso, L., Piccinini, D., Di Stefano, R., & De Gori, P. (2011). The anatomy of the 2009 L'Aquila normal fault system (central Italy) imaged by high resolution foreshock and aftershock locations. *Journal of Geophysical Research*, *116*(B12). https://doi.org/10.1029/2011JB008352

Chorowicz, J., & Sorlien, C. (1992). Oblique extensional tectonics in the Malawi Rift, Africa. The *Geological Society of America Bulletin*, *104*(8), 1015–1023. https://doi.org/10.1130/0016-7606(1992)104<1015:OETITM>2.3.CO;2

Cipollari, P., & Cosentino, D. (1995). Miocene unconformities in the Central Apennines: Geodynamic significance and sedimentary basin evolution. *Tectonophysics*, *252*(1–4), 375–389. https://doi.org/10.1016/0040-1951(95)00088-7

Clark, P. U., Dyke, A. S., Shakun, J. D., Carlson, A. E., Clark, J., Wohlfarth, B., et al. (2009). The last glacial maximum. *Science*, *325*(5941), 710–714. https://doi.org/10.1126/science.1172873

Cosentino, D., Asti, R., Nocentini, M., Gliozzi, E., Kotsakis, T., Mattei, M., et al. (2017). New insights into the onset and evolution of the central Apennine extensional intermontane basins based on the tectonically active L'Aquila Basin (central Italy). *GSA Bulletin*, *129*(9–10), 1314–1336. https://doi.org/10.1130/B31679.1

Cosentino, D., Cipollari, P., Marsili, P., & Scrocca, D. (2010). Geology of the central Apennines: A regional review. *Journal of the Virtual Explorer*, *36*(11), 1–37. https://doi.org/10.3809/jvirtex.2010.00223

Cowie, P. A., & Roberts, G. P. (2001). Constraining slip rates and spacings for active normal faults. *Journal of Structural Geology*, *23*(12), 1901–1915. https://doi.org/10.1016/S0191-8141(01)00036-0

D'Agostini, G. (2004). Asymmetric uncertainties: Sources, treatment and potential dangers. *arXiv preprint physics/0403086*. Retrieved from https://arxiv.org/abs/physics/0403086

D'Agostino, N., Giuliani, R., Mattone, M., & Bonci, L. (2001). Active crustal extension in the central Apennines (Italy) inferred from GPS measurements in the interval 1994–1999. *Geophysical Research Letters*, *28*(10), 2121–2124. https://doi.org/10.1029/2000GL012462

Delorme, A., Grandin, R., Klinger, Y., Pierrot-Deseilligny, M., Feuillet, N., Jacques, E., et al. (2019). Complex deformation at shallow depth during the 30 October 2016 *Mw*6. 5 Norcia earthquake: Interference between tectonic and gravity processes? *Tectonics*, *38*. https://doi.org/10.1029/2019TC005596

DePolo, C. M., Clark, D. G., Slemmons, D. B., & Ramelli, A. R. (1991). Historical surface faulting in the Basin and Range province, western North America: Implications for fault segmentation. *Journal of Structural Geology*, *13*(2), 123–136. https://doi.org/10.1016/0191-8141(91)90061-M

Devoti, R., Pietrantonio, G., Pisani, A. R., Riguzzi, F., & Serpelloni, E. (2010). Present day kinematics of Italy. *Journal of the Virtual Explorer*, *36*(2). https://doi.org/10.3809/jvirtex.2010.00237

Dewey, J. F., Helman, M. L., Knott, S. D., Turco, E., & Hutton, D. H. W. (1989). Kinematics of the western Mediterranean. *Geological Society, London, Special Publications*, *45*(1), 265–283. https://doi.org/10.1144/GSL.SP.1989.045.01.15

Di Luccio, F., Ventura, G., Di Giovambattista, R., Piscini, A., & Cinti, F. R. (2010). Normal faults and thrusts reactivated by deep fluids: The 6 April 2009 *Mw* 6.3 L'Aquila earthquake, central Italy. *Journal of Geophysical Research*, *115*(B6). https://doi.org/10.1029/2009JB007190

Doglioni, C., Barba, S., Carminati, E., & Riguzzi, F. (2015). Fault on-off versus strain rate and earthquakes energy. *Geoscience Frontiers*, *6*(2), 265–276. https://doi.org/10.1016/j.gsf.2013.12.007

EMERGEO Working Group. (2010). Evidence for surface rupture associated with the *Mw* 6.3 L'Aquila earthquake sequence of April 2009 (central Italy). *Terra Nova*, *22*(1), 43–51. https://doi.org/10.1111/j.1365-3121.2009.00915.x

Falcucci, E., Gori, S., Bignami, C., Pietrantonio, G., Melini, D., Moro, M., et al. (2018). The Campotosto seismic gap in between the 2009 and 2016–2017 seismic sequences of central Italy and the role of inherited lithospheric faults in regional seismotectonic settings. *Tectonics*, *37*(8), 2425–2445. https://doi.org/10.1029/2017TC004844

Falcucci, E., Gori, S., Moro, M., Pisani, A. R., Melini, D., Galadini, F., & Fredi, P. (2011). The 2009 L'Aquila earthquake (Italy): What's next in the region? Hints from stress diffusion analysis and normal fault activity. *Earth and Planetary Science Letters*, *305*(3–4), 350–358. https://doi.org/10.1016/j.epsl.2011.03.016

Ferrill, D. A., & Morris, A. P. (2001). Displacement gradient and deformation in normal fault systems. *Journal of Structural Geology*, *23*(4), 619–638. https://doi.org/10.1016/S0191-8141(00)00139-5

Fossen, H., & Rotevatn, A. (2016). Fault linkage and relay structures in extensional settings—A review. *Earth-Science Reviews*, *154*, 14–28. https://doi.org/10.1016/j.earscirev.2015.11.014

Freed, A. M. (2005). Earthquake triggering by static, dynamic, and postseismic stress transfer. *Annual Review of Earth and Planetary Sciences*, *33*, 335–367. https://doi.org/10.1146/annurev.earth.33.092203.122505

Galadini, F., Falcucci, E., Gori, S., Zimmaro, P., Cheloni, D., & Stewart, J. P. (2018). Active faulting in source region of 2016–2017 central Italy event sequence. *Earthquake Spectra*, *34*(4), 1557–1583. https://doi.org/10.1193/101317EQS204M

Galadini, F., & Galli, P. (2000). Active tectonics in the central Apennines (Italy)-input data for seismic hazard assessment. *Natural Hazards*, *22*(3), 225–268. https://doi.org/10.1023/A:1008149531980

Galderisi, A., & Galli, P. (2020). Coulomb stress transfer between parallel faults. The case of Norcia and Mt Vettore normal faults (Italy, 2016 *Mw* 6.6 earthquake). *Results in Geophysical Sciences*, (1–4), 100003. https://doi.org/10.1016/j.ringps.2020.100003

Galli, P. (2020). Recurrence times of central-southern Apennine faults (Italy): Hints from paleoseismology. *Terra Nova*, *32*, 399–407. https://doi.org/10.1111/ter.12470

Galli, P., Galadini, F., & Pantosti, D. (2008). Twenty years of paleoseismology in Italy. *Earth-Science Reviews*, *88*(1–2), 89–117. https://doi.org/10.1016/j.earscirev.2008.01.001

Galli, P., Galderisi, A., Marinelli, R., Messina, P., Peronace, E., & Polpetta, F. (2020). A reappraisal of the 1599 earthquake in Cascia (Italian Central Apennines): Hypothesis on the seismogenic source. *Tectonophysics*, *774*, 228287. https://doi.org/10.1016/j.tecto.2019.228287

Galli, P., Galderisi, A., Peronace, E., Giaccio, B., Hajdas, I., Messina, P., et al. (2019). The awakening of the dormant Mount Vettore fault (2016 central Italy earthquake, *Mw* 6.6): Paleoseismic clues on its millennial silences. *Tectonics*, *38*(2), 687–705. https://doi.org/10.1029/2018TC005326

Galli, P., Giaccio, B., Messina, P., & Peronace, E. (2016). Three magnitude 7 earthquakes on a single fault in central Italy in 1400 years, evidenced by new paleoseismic results. *Terra Nova*, *28*, 146–154. https://doi.org/10.1111/ter.12202

Galli, P., Messina, P., Giaccio, B., Peronace, E., & Quadrio, B. (2012). Early Pleistocene to late Holocene activity of the Magnola fault (Fucino fault system, central Italy). *Bollettino di Geofisica Teorica ed Applicata*, *53*(4). https://doi.org/10.4430/bgta0054

Galli, P., & Peronace, E. (2014). New paleoseismic data from the Irpinia Fault. A different seismogenic perspective for southern Apennines (Italy). *Earth-Science Reviews*, *136*, 175–201. https://doi.org/10.1016/j.earscirev.2014.05.013

Ghisetti, F., & Vezzani, L. (1996). Geometrie deformative ed evoluzione cinematica dell'Appennino centrale. *Studi Geologici Camerti*, *14*, 127–154. https://doi.org/10.15165/studgeocam-802

Giaccio, B., Galadini, F., Sposato, A., Messina, P., Moro, M., Zreda, M., et al. (2003). Image processing and roughness analysis of exposed bedrock fault planes as a tool for paleoseismological analysis: Results from the Campo Felice fault (central Apennines, Italy). *Geomorphology*, *49*(3–4), 281–301. https://doi.org/10.1016/S0169-555X(02)00191-5

Giaccio, B., Galli, P., Messina, P., Peronace, E., Scardia, G., Sottili, G., et al. (2012). Fault and basin depocentre migration over the last 2 Ma in the L'Aquila 2009 earthquake region, central Italian Apennines. *Quaternary Science Reviews*, *56*, 69–88. https://doi.org/10.1016/j.quascirev.2012.08.016

Giraudi, C. (1995). Considerations on the significance of some post-glacial fault scarps in the Abruzzo Apennines (Central Italy). *Quaternary International*, *25*, 33–45. https://doi.org/10.1016/1040-6182(94)00033-2

Giraudi, C., Bodrato, G., Lucchi, M. R., Cipriani, N., Villa, I. M., Giaccio, B., & Zuppi, G. M. (2011). Middle and late Pleistocene glaciations in the Campo Felice Basin (central Apennines, Italy). *Quaternary Research*, *75*(1), 219–230. https://doi.org/10.1016/j.yqres.2010.06.006

Giraudi, C., & Giaccio, B. (2017). Middle Pleistocene glaciations in the Apennines, Italy: New chronological data and preservation of the glacial record. *Geological Society, London, Special Publications*, *433*(1), 161–178. https://doi.org/10.1144/SP433.1

Goodall, H. J., Gregory, L. C., Wedmore, L. N. J., McCaffrey, K. J. W., Amey, R. M. J., Roberts, G. P., et al. (2021). Determining histories of slip on normal faults with bedrock scarps using cosmogenic nuclide exposure data. *Tectonics*, *40*. https://doi.org/10.1029/2020TC006457

Gori, S., Falcucci, E., Ladina, C., Marzorati, S., & Galadini, F. (2017). Active faulting, 3-D geological architecture and Plio-Quaternary structural evolution of extensional basins in the central Apennine chain, Italy. *Solid Earth*, *8*, 319–337. https://doi.org/10.5194/se-8-319-2017

Guerrieri, L., Baer, G., Hamiel, Y., Amit, R., Blumetti, A. M., Comerci, V., et al. (2010). InSAR data as a field guide for mapping minor earthquake surface ruptures: Ground displacements along the Paganica Fault during the 6 April 2009 L'Aquila earthquake. *Journal of Geophysical Research*, *115*(B12). https://doi.org/10.1029/2010JB007579

Gupta, A., & Scholz, C. H. (2000). A model of normal fault interaction based on observations and theory. *Journal of Structural Geology*, *22*(7), 865–879. https://doi.org/10.1016/S0191-8141(00)00011-0

Hanks, T. C., & Bakun, W. H. (2002). A bilinear source-scaling model for M-logA observations of continental earthquakes. *Bulletin of the Seismological Society of America*, *92*(5), 1841–1846. https://doi.org/10.1785/0120010148

Henry, C., & Das, S. (2001). Aftershock zones of large shallow earthquakes: Fault dimensions, aftershock area expansion and scaling relations. *Geophysical Journal International*, *147*, 272–293. https://doi.org/10.1046/j.1365-246X.2001.00522.x

Hunstad, I., Anzidei, M., Cocco, M., Baldi, P., Galvani, A., & Pesci, A. (1999). Modeling coseismic displacements during the 1997 Umbria-Marche earthquake (central Italy). *Geophysical Journal International*, *139*(2), 283–295. https://doi.org/10.1046/j.1365-246x.1999.00949.x

Iezzi, F., Roberts, G., & Walker, J. F. (2020). Throw-rate variations within linkage zones during the growth of normal faults: Case studies from the Western Volcanic Zone, Iceland. *Journal of Structural Geology*, *133*, 103976. https://doi.org/10.1016/j.jsg.2020.103976

Iezzi, F., Roberts, G., Walker, J. F., & Papanikolaou, I. (2019). Occurrence of partial and total coseismic ruptures of segmented normal fault systems: Insights from the Central Apennines, Italy. *Journal of Structural Geology*, *126*, 83–99. https://doi.org/10.1016/j.jsg.2019.05.003

Kanamori, H., & Brodsky, E. E. (2004). The physics of earthquakes. *Reports on Progress in Physics*, *67*(8), 1429–1496. https://doi.org/10.1088/0034-4885/67/8/R03

Kastelic, V., Burrato, P., Carafa, M. M., & Basili, R. (2017). Repeated surveys reveal nontectonic exposure of supposedly active normal faults in the central Apennines, Italy. *Journal of Geophysical Research: Earth Surface*, *122*(1), 114–129. https://doi.org/10.1002/2016JF003953

Kim, Y. S., Peacock, D. C., & Sanderson, D. J. (2004). Fault damage zones. *Journal of Structural Geology*, *26*(3), 503–517. https://doi.org/10.1016/j.jsg.2003.08.002

King, G. C., Stein, R. S., & Lin, J. (1994). Static stress changes and the triggering of earthquakes. *Bulletin of the Seismological Society of America*, *84*(3), 935–953. Retrieved from https://pubs.geoscienceworld.org/ssa/bssa/article-abstract/84/3/935/102745

Leonard, M. (2010). Earthquake fault scaling: Self-consistent relating of rupture length, width, average displacement, and moment release. *Bulletin of the Seismological Society of America*, *100*(5A), 1971–1988. https://doi.org/10.1785/0120090189

Lin, J., & Stein, R. S. (2004). Stress triggering in thrust and subduction earthquakes and stress interaction between the southern San Andreas and nearby thrust and strike-slip faults. *Journal of Geophysical Research*, *109*(B2). https://doi.org/10.1029/2003JB002607

Lunn, R. J., Willson, J. P., Shipton, Z. K., & Moir, H. (2008). Simulating brittle fault growth from linkage of preexisting structures. *Journal of Geophysical Research*, *113*(B7). https://doi.org/10.1029/2007JB005388

Malinverno, A., & Ryan, W. B. (1986). Extension in the Tyrrhenian Sea and shortening in the Apennines as result of arc migration driven by sinking of the lithosphere. *Tectonics*, *5*(2), 227–245. https://doi.org/10.1029/TC005i002p00227

Manighetti, I., Campillo, M., Bouley, S., & Cotton, F. (2007). Earthquake scaling, fault segmentation, and structural maturity. *Earth and Planetary Science Letters*, *253*(3–4), 429–438. https://doi.org/10.1016/j.epsl.2006.11.004

Mann, H. B., & Wald, A. (1942). On the choice of the number of class intervals in the application of the chi square test. *The Annals of Mathematical Statistics*, *13*(3), 306–317. https://doi.org/10.1214/aoms/1177731569. Retrieved from https://www.jstor.org/stable/i312731

McClay, K., & Khalil, S. (1998). Extensional hard linkages, eastern Gulf of Suez, Egypt. *Geology*, *26*(6), 563–566. https://doi.org/10.1130/00917613(1998)026<0563:EHLEGO>2.3.CO;2

McGrath, A. G., & Davison, I. (1995). Damage zone geometry around fault tips. *Journal of Structural Geology*, *17*(7), 1011–1024. https://doi.org/10.1016/0191-8141(94)00116-H

Meng, L., Ampuero, J. P., Stock, J., Duputel, Z., Luo, Y., & Tsai, V. C. (2012). Earthquake in a maze: Compressional rupture branching during the 2012 *Mw* 8.6 Sumatra earthquake. *Science*, *337*(6095), 724–726. https://doi.org/10.1126/science.1224030

Mercuri, M., McCaffrey, K. J., Smeraglia, L., Mazzanti, P., Collettini, C., & Carminati, E. (2020). Complex geometry and kinematics of subsidiary faults within a carbonate-hosted relay ramp. *Journal of Structural Geology*, *130*, 103915. https://doi.org/10.1016/j.jsg.2019.103915

Mignan, A., Danciu, L., & Giardini, D. (2015). Reassessment of the maximum fault rupture length of strike-slip earthquakes and inference on M max in the Anatolian Peninsula, Turkey. *Seismological Research Letters*, *86*(3), 890–900. https://doi.org/10.1785/0220140252

Montone, P., Mariucci, M. T., Pondrelli, S., & Amato, A. (2004). An improved stress map for Italy and surrounding regions (central Mediterranean). *Journal of Geophysical Research*, *109*(B10). https://doi.org/10.1029/2003JB002703

Morell, K. D., Styron, R., Stirling, M., Griffin, J., Archuleta, R., & Onur, T. (2020). Seismic hazard analyses from geologic and geomorphic data: Current and future challenges. *Tectonics*, *39*(10), e2018TC005365. https://doi.org/10.1029/2018TC005365

Morewood, N. C., & Roberts, G. P. (2000). The geometry, kinematics and rates of deformation within an en échelon normal fault segment boundary, central Italy. *Journal of Structural Geology*, *22*(8), 1027–1047. https://doi.org/10.1016/S0191-8141(00)00030-4

Moustafa, A. R. (2002). Controls on the geometry of transfer zones in the Suez rift and northwest Red Sea: Implications for the structural geometry of rift systems. *AAPG Bulletin*, *86*(6), 979–1002. https://doi.org/10.1306/61EEDC06-173E-11D7-8645000102C1865D

Nicol, A., Mouslopoulou, V., Begg, J., & Oncken, O. (2020). Displacement accumulation and sampling of paleoearthquakes on active normal faults of Crete in the eastern Mediterranean. *Geochemistry, Geophysics, Geosystems*, *21*(11), e2020GC009265. https://doi.org/10.1029/2020GC009265

Nocentini, M., Asti, R., Cosentino, D., Durante, F., Gliozzi, E., Macerola, L., & Tallini, M. (2017). Plio-Quaternary geology of L'Aquila–Scoppito Basin (Central Italy). *Journal of Maps*, *13*(2), 563–574. https://doi.org/10.1080/17445647.2017.1340910

Okada, Y. (1992). Internal deformation due to shear and tensile faults in a half-space. *Seismical Society of America*, *82*, 1018–1040. Retrieved from http://citeseerx.ist.psu.edu/viewdoc/download?doi=10.1.1.484.8168&rep=rep1&type=pdf

Pace, B., Boncio, P., & Lavecchia, G. (2002). The 1984 Abruzzo earthquake (Italy): An example of seismogenic process controlled by interaction between differently oriented synkinematic faults. *Tectonophysics*, *350*(3), 237–254. https://doi.org/10.1016/S0040-1951(02)00118-X

Pantosti, D., D'Addezio, G., & Cinti, F. R. (1996). Paleoseismicity of the Ovindoli-Pezza fault, central Apennines, Italy: A history including a large, previously unrecorded earthquake in the Middle Ages (860–1300 AD). *Journal of Geophysical Research*, *101*(B3), 5937–5959. https://doi.org/10.1029/95JB03213

Papadopoulos, G. A., & Minadakis, G. (2016). Foreshock patterns preceding great earthquakes in the subduction zone of Chile. In *Geodynamics of the Latin American Pacific Margin* (pp. 3247–3271). Birkhäuser. https://doi.org/10.1007/978-3-319-51529-8_3

Papanikolaou, I. D., Roberts, G. P., & Michetti, A. M. (2005). Fault scarps and deformation rates in Lazio–Abruzzo, Central Italy: Comparison between geological fault slip-rate and GPS data. *Tectonophysics*, *408*(1–4), 147–176. https://doi.org/10.1016/j.tecto.2005.05.043

Peacock, D. C. P. (2002). Propagation, interaction and linkage in normal fault systems. *Earth-Science Reviews*, *58*(1–2), 121–142. https://doi.org/10.1016/S0012-8252(01)00085-X

Peacock, D. C. P., Nixon, C. W., Rotevatn, A., Sanderson, D. J., & Zuluaga, L. F. (2017). Interacting faults. *Journal of Structural Geology*, *97*, 1–22. https://doi.org/10.1016/j.jsg.2017.02.008

Peacock, D. C. P., & Sanderson, D. J. (1991). Displacements, segment linkage and relay ramps in normal fault zones. *Journal of Structural Geology*, *13*(6), 721–733. https://doi.org/10.1016/0191-8141(91)90033-F

Peacock, D. C. P., & Sanderson, D. J. (1994). Geometry and development of relay ramps in normal fault systems. *AAPG Bulletin*, *78*(2), 147–165. https://doi.org/10.1306/BDFF9046-1718-11D7-8645000102C1865D

Pucci, S., De Martini, P. M., Civico, R., Villani, F., Nappi, R., Ricci, T., et al. (2017). Coseismic ruptures of the 24 August 2016, *Mw* 6.0 Amatrice earthquake (central Italy). *Geophysical Research Letters*, *44*(5), 2138–2147. https://doi.org/10.1002/2016GL071859

Pucci, S., Villani, F., Civico, R., Di Naccio, D., Porreca, M., Benedetti, L., et al. (2019). Complexity of the 2009 L'Aquila earthquake causative fault system (Abruzzi Apennines, Italy) and effects on the Middle Aterno Quaternary basin arrangement. *Quaternary Science Reviews*, *213*, 30–66. https://doi.org/10.1016/j.quascirev.2019.04.014

Reches, Z. E., & Dewers, T. A. (2005). Gouge formation by dynamic pulverization during earthquake rupture. *Earth and Planetary Science Letters*, *235*(1–2), 361–374. https://doi.org/10.1016/j.epsl.2005.04.009

Romanowicz, B., & Ruff, L. J. (2002). On moment-length scaling of large strike slip earthquakes and the strength of faults. *Geophysical Research Letters*, *29*(12). https://doi.org/10.1029/2001GL014479

Rotevatn, A., & Peacock, D. C. (2018). Strike-slip reactivation of segmented normal faults: Implications for basin structure and fluid flow. *Basin Research*, *30*(6), 1264–1279. https://doi.org/10.1111/bre.12303

Rovida, A. N., Locati, M., Camassi, R. D., Lolli, B., & Gasperini, P. (2016). *CPTI15, the 2015 version of the parametric catalogue of Italian earthquakes*. Retrieved from https://www.earth-prints.org/bitstream/2122/10585/2/CPTI15_descrizione.pdf

Salvi, S., Cinti, F. R., Colini, L., D'addezio, G., Doumaz, F., & Pettinelli, E. (2003). Investigation of the active Celano–L'Aquila fault system, Abruzzi (central Apennines, Italy) with combined ground-penetrating radar and paleoseismic trenching. *Geophysical Journal International*, *155*(3), 805–818. https://doi.org/10.1111/j.1365-246X.2003.02078.x

Schlagenhauf, A., Manighetti, I., Benedetti, L., Gaudemer, Y., Finkel, R., Malavieille, J., & Pou, K. (2011). Earthquake supercycles in Central Italy, inferred from 36Cl exposure dating. *Earth and Planetary Science Letters*, *307*(3–4), 487–500. https://doi.org/10.1016/j.epsl.2011.05.022

Schlische, R. W., Young, S. S., Ackermann, R. V., & Gupta, A. (1996). Geometry and scaling relations of a population of very small rift-related normal faults. *Geology*, *24*(8), 683. https://doi.org/10.1130/0091-7613(1996)024<0683:gasroa>2.3.co;2

Scholz, C. H. (2010). Large earthquake triggering, clustering, and the synchronization of faults. *Bulletin of the Seismological Society of America*, *100*(3), 901–909. https://doi.org/10.1785/0120090309

Scognamiglio, L., Tinti, E., Casarotti, E., Pucci, S., Villani, F., Cocco, M., et al. (2018). Complex fault geometry and rupture dynamics of the *MW* 6.5, 30 October 2016, Central Italy earthquake. *Journal of Geophysical Research: Solid Earth*, *123*(4), 2943–2964. https://doi.org/10.1002/2018JB015603

Scognamiglio, L., Tinti, E., Michelini, A., Dreger, D. S., Cirella, A., Cocco, M., et al. (2010). Fast determination of moment tensors and rupture history: What has been learned from the 6 April 2009 L'Aquila earthquake sequence. *Seismological Research Letters*, *81*(6), 892–906. https://doi.org/10.1785/gssrl.81.6.892

Scotti, O., Visini, F., Faure Walker, J., Peruzza, L., Pace, B., Benedetti, L., et al. (2021). Which fault threatens me most? Bridging the gap between geologic data-providers and seismic risk practitioners. *Frontiers of Earth Science*, *8*, 750. https://doi.org/10.3389/feart.2020.626401

Servizio Geologico d'Italia-APAT. (2004). *Foglio 368 "Avezzano" della Carta Geologica d'Italia alla scala 1:50.000*. Retrieved from http://www.isprambiente.gov.it/Media/carg/368_AVEZZANO/Foglio.html

Servizio Geologico d'Italia-APAT. (2006). *Foglio 359 "L'Aquila" della Carta Geologica d'Italia alla scala 1:50,000*. Retrieved from http://www.isprambiente.gov.it/Media/carg/359_LAQUILA/Foglio.html

Servizio Geologico d'Italia-APAT. (2010). *Foglio 358 "Pescorocchiano" della Carta Geologica d'Italia alla scala 1:50,000*. Retrieved from http://www.isprambiente.gov.it/Media/carg/358_PESCOROCCHIANO/Foglio.html

Sgambato, C., Walker, J. P. F., Mildon, Z. K., & Roberts, G. P. (2020). Stress loading history of earthquake faults influenced by fault/shear zone geometry and Coulomb pre-stress. *Scientific Reports*, *10*(1), 1–10. https://doi.org/10.1038/s41598-020-69681-w

Smeraglia, L., Billi, A., Carminati, E., Cavallo, A., & Doglioni, C. (2017). Field- to nano-scale evidence for weakening mechanisms along the fault of the 2016 Amatrice and Norcia earthquakes, Italy. *Tectonophysics*, *712713*, 156–169. https://doi.org/10.1016/j.tecto.2017.05.014

Spina, V., Tondi, E., Galli, P., & Mazzoli, S. (2009). Fault propagation in a seismic gap area (northern Calabria, Italy): Implications for seismic hazard. *Tectonophysics*, *476*(1–2), 357–369. https://doi.org/10.1016/j.tecto.2009.02.001

Spina, V., Tondi, E., Galli, P., Mazzoli, S., & Cello, G. (2008). Quaternary fault segmentation and interaction in the epicentral area of the 1561 earthquake (*Mw* = 6.4), Vallo di Diano, southern Apennines, Italy. *Tectonophysics*, *453*(1–4), 233–245. https://doi.org/10.1016/j.tecto.2007.06.012

Stein, R. S. (2003). Earthquake conversations. *Scientific American*, *288*(1), 72–79. https://doi.org/10.1038/scientificamerican0103-72

Stein, R. S., Barka, A. A., & Dieterich, J. H. (1997). Progressive failure on the North Anatolian fault since 1939 by earthquake stress triggering. *Geophysical Journal International*, *128*(3), 594–604. https://doi.org/10.1111/j.1365-246X.1997.tb05321.x

Toda, S., Stein, R. S., Sevilgen, V., & Lin, J. (2011). Coulomb 3.3 graphic-rich deformation and stress-change software for earthquake, tectonic, and volcano research and teaching-user guide (No. 2011-1060). *US Geological Survey*. https://doi.org/10.3133/ofr20111060

Tondi, E., & Cello, G. (2003). Spatiotemporal evolution of the Central Apennines fault system (Italy). *Journal of Geodynamics*, *36*(1–2), 113–128. https://doi.org/10.1016/S0264-3707(03)00043-7

Tondi, E., Jablonská, D., Volatili, T., Michele, M., Mazzoli, S., & Pierantoni, P. P. (2020). The Campotosto linkage fault zone between the 2009 and 2016 seismic sequences of central Italy: Implications for seismic hazard analysis. *GSA Bulletin*. https://doi.org/10.1130/B35788.1

Tortorici, G., Romagnoli, G., Grassi, S., Imposa, S., Lombardo, G., Panzera, F., & Catalano, S. (2019). Quaternary negative tectonic inversion along the Sibillini Mts. thrust zone: The Arquata del Tronto case history (Central Italy). *Environmental Earth Sciences*, *78*(1), 37. https://doi.org/10.1007/s12665-018-8021-2

Trippetta, F., Petricca, P., Billi, A., Collettini, C., Cuffaro, M., Lombardi, A. M., et al. (2019). From mapped faults to fault-length earthquake magnitude (FLEM): A test on Italy with methodological implications. *Solid Earth*, *10*, 1555–1579. https://doi.org/10.5194/se-10-1555-2019

Trudgill, B., & Cartwright, J. (1994). Relay-ramp forms and normal-fault linkages, Canyonlands National Park, Utah. *The Geological Society of America Bulletin*, *106*(9), 1143–1157. https://doi.org/10.1130/0016-7606(1994)106<1143:RRFANF>2.3.CO;2

Tung, S., & Masterlark, T. (2018). Delayed poroelastic triggering of the 2016 October Visso earthquake by the August Amatrice earthquake, Italy. *Geophysical Research Letters*, *45*(5), 2221–2229. https://doi.org/10.1002/2017GL076453

Villani, F., Civico, R., Pucci, S., Pizzimenti, L., Nappi, R., De Martini, P. M. (2018). A database of the coseismic effects following the 30 October 2016 Norcia earthquake in Central Italy. *Scientific Data*, *5*, 180049. https://doi.org/10.1038/sdata.2018.49

Villani, F., Tulliani, V., Sapia, V., Fierro, E., Civico, R., & Pantosti, D. (2015). Shallow subsurface imaging of the Piano di Pezza active normal fault (central Italy) by high-resolution refraction and electrical resistivity tomography coupled with time-domain electromagnetic data. *Geophysical Supplements to the Monthly Notices of the Royal Astronomical Society*, *203*(3), 1482–1494. https://doi.org/10.1093/gji/ggv399

Walker, J. F., Boncio, P., Pace, B., Roberts, G., Benedetti, L., Scotti, O., et al. (2021). Fault2SHA Central Apennines database and structuring active fault data for seismic hazard assessment. *Scientific Data*, *8*(1), 1–20. https://doi.org/10.1594/PANGAEA.922582

Walker, J. F., Roberts, G. P., Cowie, P. A., Papanikolaou, I. D., Sammonds, P. R., Michetti, A. M., & Phillips, R. J. (2009). Horizontal strain-rates and throw-rates across breached relay zones, central Italy: Implications for the preservation of throw deficits at points of normal fault linkage. *Journal of Structural Geology*, *31*(10), 1145–1160. https://doi.org/10.1016/j.jsg.2009.06.011

Walsh, J. J., & Watterson, J. (1991). Geometric and kinematic coherence and scale effects in normal fault systems. *Geological Society, London, Special Publications*, *56*(1), 193–203. https://doi.org/10.1144/GSL.SP.1991.056.01.13

Walsh, J. J., Watterson, J., Bailey, W. R., & Childs, C. (1999). Fault relays, bends and branch-lines. *Journal of Structural Geology*, *21*(8–9), 1019–1026. https://doi.org/10.1016/S0191-8141(99)00026-7

Wells, D. L., & Coppersmith, K. J. (1994). New empirical relationships among magnitude, rupture length, rupture width, rupture area, and surface displacement. *Bulletin of the Seismological Society of America*, *84*(4), 974–1002. Retrieved from https://pubs.geoscienceworld.org/ssa/bssa/article-abstract/84/4/974/119792/New-empirical-relationships-among-magnitude?redirectedFrom=fulltext

Wesnousky, S. G. (2008). Displacement and geometrical characteristics of earthquake surface ruptures: Issues and implications for seismic-hazard analysis and the process of earthquake rupture. *Bulletin of the Seismological Society of America*, *98*(4), 1609–1632. https://doi.org/10.1785/0120070111

Wilkinson, M., Roberts, G. P., McCaffrey, K., Cowie, P. A., Walker, J. P. F., Papanikolaou, I., et al. (2015). Slip distributions on active normal faults measured from LiDAR and field mapping of geomorphic offsets: An example from L'Aquila, Italy, and implications for modeling seismic moment release. *Geomorphology*, *237*, 130–141. https://doi.org/10.1016/j.geomorph.2014.04.026

Williams, G., & Chapman, T. (1983). Strains developed in the hangingwalls of thrusts due to their slip/propagation rate: A dislocation model. *Journal of Structural Geology*, *5*(6), 563–571. https://doi.org/10.1016/0191-8141(83)90068-8

Xu, W., Feng, G., Meng, L., Zhang, A., Ampuero, J. P., Bürgmann, R., & Fang, L. (2018). Transpressional rupture cascade of the 2016 *Mw* 7.8 Kaikoura earthquake, New Zealand. *Journal of Geophysical Research: Solid Earth*, *123*(3), 2396–2409. https://doi.org/10.1002/2017JB015168

Zhang, P., Slemmons, D. B., & Mao, F. (1991). Geometric pattern, rupture termination and fault segmentation of the Dixie Valley—Pleasant Valley active normal fault system, Nevada, USA. *Journal of Structural Geology*, *13*(2), 165–176. https://doi.org/10.1016/0191-8141(91)90064-P